האוניברסיטה העברית בירושלים
The Hebrew University of Jerusalem

הפקולטה למתמטיקה ולמדעי הטבע

בית הספר להנדסה ומדעי המחשב

המחלקה לפיסיקה יישומית

עבודת גמר לקראת תואר מוסמך M.Sc

בנושא:

ניתוח הכוח האופטי במערכת של מיקרו- מהוד טבעתי

Analysis of the optical force in the Micro Ring Resonator

מוגש על ידי: אביגדור עינת

בהנחיית: פרופסור אוריאל לוי

אלול התשע"א

September 2011

עבודה זו מוקדשת למשפחתי, התומכת בי לאורך הדרך:

בתודה להוריי שהבעירו בי את אש הדעת והסקרנות,

ובהכרת הטוב ליפעת שבעזרתה אש זו עודנה בוערת.

בתפילה לבורא עולם שיתקיים בנו:

"רבי חנניה בן דוסא אומר, כל שיראת חטאו קודמת לחכמתו, חכמתו מתקיימת;
וכל שחכמתו קודמת ליראת חטאו, אין חכמתו מתקיימת (אבות, ג', י"א)".

Acknowledgements

I would like to thank my supervisor Prof. Uriel Levy. His guidance and assistance made this work possible.

Thanks to all members of the Nano-Opto laboratory for their help and support. I would like to thank in particular to Raviv Yitzhaki, Boris Desiatov, and Ilya Goykhman for fruitful discussions.

Abstract

This thesis is devoted to the investigation of the optical force in a micro ring resonator. The research consists of an analytical model based on the coupled mode theory as well as on numerical calculations based on the finite element method. Our model shows that the resonance enhancement of the force is diminished by the opposing contributions of the attractive and the repulsive forces related to the symmetric and the anti symmetric modes in the coupling region. We show that this limiting factor can be removed by adding asymmetry to the system, e.g. by modifying one of the waveguides. In addition, we study the combination of a micro ring resonator coupled to a one dimensional photonic crystal waveguide. This modified geometry allows further enhancement of the optical force via the combination of optical resonances and slow light effect.

Contents

1. Introduction

This chapter will present the scientific discipline in which the thesis deals with. Specifically, a short review on the scientific achievements in optomechanical devices, using the gradient optical force will be given. After these two necessary backgrounds, the motivation for the research described in the thesis will be given.

1.1. Nano-photonics

21st-century society requires new optical science and technology to meet the measurement, fabrication, control, and function-requirements on the scale of the microelectronic chips, which are several tens of nanometers. This requirement is in view of the well known fact that conventional optical science and technology cannot overcome the diffraction limit of light waves. The scientific field which is aimed to give the answer is nano-photonics.

Nano-photonics deals with the interaction of light and matter, where the typical dimensions of the structures are in the order of or smaller than the optical wavelength. The behavior of the light in this case is rich and unexpected, and can be treated with both the classical description of the light via Maxwell's theory and the quantum field theory for the light and the matter's features. This scientific field is young and developing since the nanofabrication capabilities (which are generally imported from the massive micro-electronics world), are only now allowing exploring this subject. In addition, the theoretical research is also developing due to the vast improvement in computation power which enables solving complex problems numerically in a way that was not possible in the past.

1.2. Optomechanical devices

As Maxwell showed in his classical theory from 1873, the electromagnetic (EM) radiation field carries momentum. Over the years, a lot of work has been done

regarding the momentum transfer between light and matter. The invention of the Laser had an enormous impact on this research due to the laser's large amount of photons per beam area as well as the beam coherence and its small diverging angle.

Specifically, in the recent years the so-called Gradient Optical Force (GOF) has been explored in the context of nano-photonic devices. The advancement in nano-fabrication capabilities, providing additional mechanical degrees of freedom, promoted the theoretical and experimental efforts in this field of research. This is a result of two reasons: 1- The force becomes dominant when the optical modes shrink to the nanometer dimensions. 2- The objects feeling the force are small enough to experience significant movement. A comprehensive review describing the topic of optomechanical device actuation through the gradient optical force can be found in [1].

Several papers performed a theoretical study of the forces between waveguide (WG) structures in various configurations and investigated several potential applications [2-21]. Perhaps the most basic work amongst these is [4]. This paper presented the idea of bonding between two rectangular strip WGs when they are free to move (see Figure 1.1), and calculated the power that is needed to cause certain deflections of the WGs. Another interesting work is presented in [7], where two vertically separated ring resonators are suggested as a device for creating optomechanical potential wells.

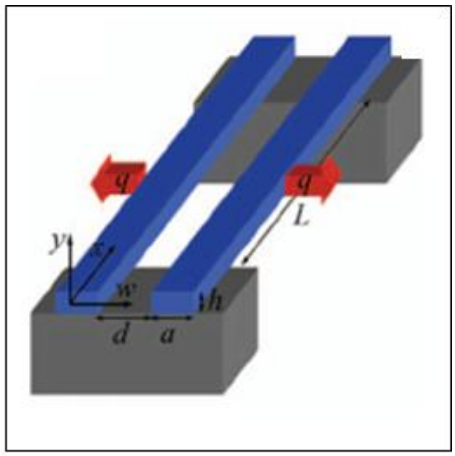

Figure 1.1: schematic of suspended section of two coupled WGs. The picture is taken from ref. [4]

The GOF was measured and characterized experimentally in numerous WG configurations, including single WG coupled to a substrate and Mach-Zender interferometers [22-25].

A recent effort is devoted to the study of the GOF in photonic resonators, for two major reasons: 1 – The GOF is resonantly enhanced via the mechanism of EM field enhancement at resonance. 2 – The narrow spectral line of photonic resonators allows substantial tuning of the optical transmission by applying GOF. For example, transmission tuning via the enhancement of the GOF was demonstrated using double ring structures [26-28] and micro disk resonators [29-30].

Significant enhancement in the GOF and transmission tuning can be also obtained in Photonic Crystals (PhC) systems by exploiting the dispersion of the band diagram and the slow light effect [31-37].

1.3. Goal of the research

This thesis studies the opto-mechanical effect in the system of the Micro Ring Resonator (MRR). More specifically, we explore the force that acts on a free standing bus WG as a result of the circulating light in the resonator. Schematic picture of the investigated structure is given in Figure 1.2

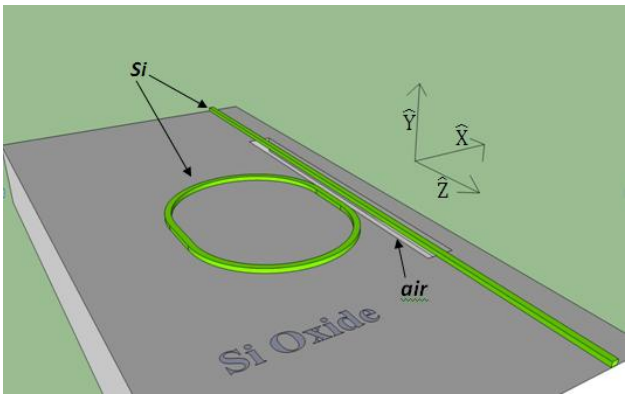

Figure 1.2: Schematic diagram of the investigated structure. The system consists of an MRR coupled to a bus WG. The substrate under the bus WG is etched to create a free standing mechanical beam. For simplicity we assumed a silicon-on-insulator (SOI) structure. However, the analysis is not restricted to this specific material platform.

Based on previous works, we use the Coupled Mode Theory (CMT) to develop a new model which provides better understanding of the GOF in the vicinity of the resonance. The model shows that as long as the bus WG and the MRR WG are identical, both the attractive (symmetric) and the repulsive (anti-symmetric) forces will be present at resonance, and thus the resonant enhancement of the GOF will be diminished. Based on this result, we numerically show that the force cancelation can be overcome by modifying one of the WGs, such that the relative phase between the two WGs at resonance can be controlled. Furthermore, we consider a novel configuration allowing further enhancement of the GOF by the coupling of an MRR to a bus WG composed of a 1-D PhC.

The thesis is organized as follows: in chapter 2 we introduce few essential theoretical backgrounds. These include the basics of the optical force and the ways for calculating it, the concept of the MRR, and a brief outline of the PhC and slow light phenomenon. Chapter 3 is devoted to an analytical general treatment of the GOF in the MRR via a CMT. In chapter 4 we turn to the numerical simulations of specific geometries. First, we present the simulations and assumptions which set the numerical frame. Secondly, we discuss our simulations in different cases, which approve the analytical model and extend it in order to get better results. The last part of this chapter is devoted to the multipart simulations which combine the mechanical and the EM degrees of freedom. These simulations predict the behavior of the actual device. Chapter 5 introduces the idea of combining 1d-PhC WG and the MRR to further increase the GOF. The chapter begins with examination of the connection between the GOF and the slow light effect. Chapter 6 concludes the thesis.

2. Theoretical background

This chapter presents the theory of three "building blocks" of the thesis- the optical force, the MRR and the PhC.

2.1. The optical force

In the following we introduce the basics of the optical force, and more specifically the GOF, and present few ways of calculating it.

2.1.1 Nature of the optical force

As was previously mentioned, the EM radiation field carries momentum within it. Whenever a physical body interacts with the EM field, this momentum is translated to an EM force acting on the body. One can see it as a generalization of the basic Lorentz force for the single charge in the EM field. The name "optical force" is used when the EM field is excited in the optical regime, obviously.

It is common [1] to distinguish between two major categories- scattering force and gradient force. While the first one, known also as radiation pressure, is the momentum that the photons transfer to the body when impinging on it, i.e. this is an axial force (directed along the radiation propagation direction), the gradient force is directed perpendicular to the radiation propagation direction. As an intuitive and incomplete explanation for its physical nature, one can use the concepts of laser trapping: The dipoles inside the dielectric body feel different force spatially, since there is a variation of the EM field in space (see Figure 2.1). By that, the body will be attracted to the spatial spot with the maximal field gradient.

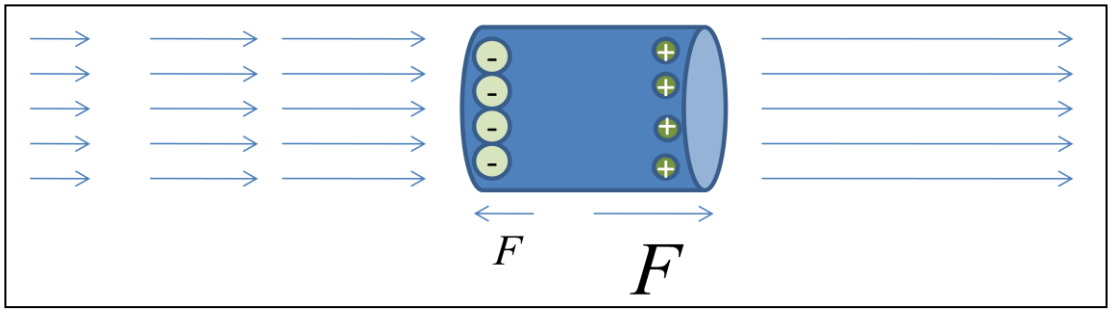

Figure 2.1: a dielectric object in a spatially varying electric field experiences total force.

Referring to the practical question of calculating the force, two extreme cases can be treated easily: 1– If the body experiencing the force is much larger than the optical wavelength the problem can be solved using the ray optics method (by considerations of reflectance and transmission). 2– If the body is much smaller than the wavelength it can be treated as a dipole in an EM field. In the intermediate cases, few methods can be applied. In the following we will present two of them.

2.1.2 The Maxwell Stress Tensor (MST) method:

The MST method is a general method of calculating the force acting on an arbitrary object in an EM field, based on Maxwell's equations. The method does not distinguish between different forces (i.e. radiation pressure, gradient, absorption, scattering), and the specific force is categorized according to the situation. For example, if the examined object has an infinitely extended planar interface and the field is a monochromatic plane wave, the result will be the classical radiation pressure. On the other hand, an MST calculation for the case of a single dipole in an EM field generates the gradient and the scattering forces, known in the laser trapping. For our geometry the obtained force is naturally of a gradient nature. In the following we will briefly review this method, and more detailed treatment can be found elsewhere [38].

We take Lorentz law for a particle with charge q and velocity $\vec{v}$:

(2.1) $$\vec{F} = q\left[\vec{E} + \vec{v} \times \vec{B}\right]$$

$$= \int_V [\rho(\vec{r},t)\vec{E}(\vec{r},t) + \vec{j}(\vec{r},t) \times \vec{B}(\vec{r},t)]dV \ .$$

Where $\vec{E}, \vec{B}$ are the electric field and the magnetic induction, and $\rho, \vec{j}$ are the charge and current distributions, respectively. Plugging in the Maxwell equations and doing some algebra leads to the following equation for the force $\vec{F}$ exerted on a body inside a volume V:

(2.2) $$\vec{F} = \varepsilon_0 \int_V [\vec{E}(\vec{\nabla} \cdot \vec{E}) - \vec{E} \times (\vec{\nabla} \times \vec{E}) + c^2 \vec{B}(\vec{\nabla} \cdot \vec{B}) - c^2 \vec{B} \times (\vec{\nabla} \times \vec{B})] dV - \frac{d}{dt} \int_V \varepsilon_0 (\vec{E} \times \vec{B}) dV \ .$$

Here, c stands for the vacuum velocity of light. After identifying the second integrand as proportional to the Pointing vector ($\frac{\int \vec{E} \times \vec{H}}{c^2} = \frac{\int \vec{S}}{c^2} \equiv \vec{P}_{field}$, "Abraham density") and doing some algebra to establish the equation as a continuity equation, we can state:

(2.3) $$\vec{F} + \frac{d}{dt} \vec{P}_{field} = \oint_S \sum_\beta \overleftrightarrow{T}_{\alpha\beta} \cdot \vec{n}_\beta \, da \ .$$

Where we define the Maxwell Stress Tensor (MST):

(2.4) $$\overleftrightarrow{T}_{\alpha\beta} = \varepsilon_0 \left[E_\alpha E_\beta + c^2 B_\alpha B_\beta - \tfrac{1}{2} \left(\vec{E} \cdot \vec{E} + c^2 \vec{B} \cdot \vec{B} \right) \delta_{\alpha\beta} \right] =$$

$$\begin{bmatrix} \frac{1}{2}\varepsilon_0 \left({E_x}^2 - {E_y}^2 - {E_z}^2 \right) + \frac{1}{2}\mu_0 \left({H_x}^2 - {H_y}^2 - {H_z}^2 \right) & \varepsilon_0 E_x E_y + \mu_0 H_x H_y & \varepsilon_0 E_x E_z + \mu_0 H_x H_z \\ \varepsilon_0 E_x E_y + \mu_0 H_x H_y & \frac{1}{2}\varepsilon_0 \left({E_y}^2 - {E_x}^2 - {E_z}^2 \right) + \frac{1}{2}\mu_0 \left({H_y}^2 - {H_x}^2 - {H_z}^2 \right) & \varepsilon_0 E_y E_z + \mu_0 H_y H_z \\ \varepsilon_0 E_x E_z + \mu_0 H_x H_z & \varepsilon_0 E_y E_z + \mu_0 H_y H_z & \frac{1}{2}\varepsilon_0 \left({E_z}^2 - {E_y}^2 - {E_x}^2 \right) + \frac{1}{2}\mu_0 \left({H_z}^2 - {H_y}^2 - {H_x}^2 \right) \end{bmatrix} .$$

(The magnetic induction was converted to magnetic field).

Thus, for a chosen volume, the mechanical force plus the temporal change in the field momentum are equal to a surface integral of the normal components of momentum "flow", which is expressed by the MST integration.

In other words, one component of the MST, $\overline{\mathrm{T}}_{\alpha\beta}$, is the $\hat{\alpha}$ component force (per area) acting on the surface perpendicular to $\hat{\beta}$. Therefore, the recipe to calculate a specific force component acting on a body in the presence of an EM field is: 1 - calculating first the MST according to the fields. 2 - Integrating the 3 relevant MST components on the 3 corresponding surfaces. 3- Adding them up.

It is crucial to mention that the fields in the calculation are not the excitation fields but rather the self consistent solutions of the problem. It means that these fields include both the excitation field as well as the scattering fields.

Let us also remind that if the fields are oscillating harmonically, one can use time averaging over one period, which results in:

(2.5) $\langle F_\alpha \rangle = \oint_s \sum_\beta \langle \overleftrightarrow{T}_{\alpha\beta}(\vec{r},t) \rangle \cdot \vec{n}_\beta \, da$.

2.1.3 The method of virtual displacement

Other way of dealing with the optical force is somewhat more elegant, and it is similar to the general method of virtual work or virtual displacement. Here we will present two approaches using this principal.

As was already mentioned, ref. [4] discussed the basic structure of two rectangular WG, separated in the horizontal direction by a gap of width ρ. The GOF was calculated in the following way:

The energy associated with an eigenmode having a frequency ω and a wave vector $\vec{k}$ is $U = N\hbar\omega$. N stands for the number of photons and $\hbar$ is the Planck constant. An adiabatic change in the separation $\Delta\rho$, shifts the eigenmode frequency by $\Delta\omega$, provided that we keep the momentum $\vec{k}$ to be constant. From energy conservation we can conclude:

(2.6) $F = -\frac{dU}{d\rho} = -\frac{d(N\hbar\omega)}{d\rho}\Big|_{\vec{k}} = -\frac{1}{\omega}\frac{d\omega}{d\rho}\Big|_{\vec{k}} \cdot U$.

This simple formula was shown in the mentioned paper to give identical results to the MST method, and in some cases it requires much less computational effort than the MST.

As others easily showed [9], one can use the relation $\omega = \frac{c \cdot |\vec{k}|}{n_{eff}}$ to get different formulation of the same equation:

(2.7) $F = \frac{1}{n_{eff}}\frac{dn_{eff}}{d\rho}\Big|_{\omega} \cdot U$.

Here, n_{eff} is the obtained effective refractive index of the optical WG. This latter result is slightly friendlier than equation **(2.6)** since the relation $n_{eff}(\rho)$ is an easy one to extract.

The work described in [14] has extended this method. This manuscript has shown that given a certain system's response in terms of the phase shift that an input signal is experiencing while interacting with the system, $\phi(q,\omega)$ (where q is a canonical degree of freedom), the optical force can be computed via the following formula:

(2.8) $$F = \Phi \cdot \hbar \cdot \frac{d\phi(q,\omega)}{dq}\Big|_{\omega} .$$

Here, Φ is the photon flux in the system. The analysis is assuming loss-less and reflection-less system having a single input and single output (although the researchers claim that the method can be expanded to more complex structures). The previous results referring to the double WG system are easily derived from this equation, while more complex systems also can be investigated using this method.

2.1.4 Method of calculation in our work:

In our work we choose to work with the more classical MST method by computing the total EM field. This is due to two reasons:

1– In a numerical frame as we are going to use it is easier to set the geometry and then to scan over the wavelength (and doing this procedure for few selected gaps) rather than scanning over the geometrical parameters for a selected wavelength.

2– Moreover, for the mechanical-EM combination it is necessary to give a fixed value of the force at a given situation (i.e. given geometry, and given incident power and wavelength), which is possible in the MST method but not in the virtual displacement method that requires calculations of other geometries to give the force for a particular geometry.

2.2. The micro ring resonator

The micro ring resonator (MRR) is a basic element in photonics. Its applications include for example all-optical switching, electro-optical switching, wavelength conversion, filtering, sensing, and reconfigurable optical delay lines. It consists of a WG in a closed loop (which is essentially the optical resonator) coupled to one or more input/output ("bus") WGs. In our work we will deal with the one bus configuration. The principle of operation is based on constructive interference of the optical signal in the ring.

To give a short theoretical description of the MRR operation, we follow a basic treatment given in [39]. Referring to Figure 2.2, one can generally state:

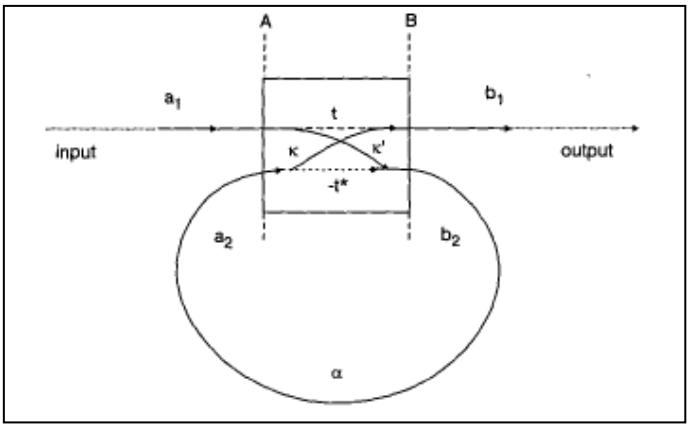

Figure 2.2: schematic picture of the MRR. The input signal, indicated as a_1, is coupled to the MRR WG, indicated as number 2. The coupling region, together with the coupling coefficients, is indicated by the square. The picture is taken from ref. [39].

(2.9) $$\begin{bmatrix} b_1 \\ b_2 \end{bmatrix} = \begin{bmatrix} t & \kappa \\ -\kappa^* & t^* \end{bmatrix} \begin{bmatrix} a_1 \\ a_2 \end{bmatrix}$$

Here, the a's and b's are the modes' complex amplitudes. The assumptions are that no losses occur in the coupling area and a single unidirectional mode of the WGs is excited. Both of the assumptions apply in our case.

The coupling coefficients (which are complex, i.e. include phase and amplitude information: $t = |t|e^{i\phi}$) are general at this point (although one optional specific description of the coupling will be described later) and they are related through:

(2.10) $|t|^2 + |\kappa|^2 = 1$

For the closed loop we can write:

(2.11) $a_2 = \alpha e^{-i\theta} b_2$

In other words, the signal changes its amplitude and its phase while propagating in the ring. The case of lossless ring, $\alpha = 1$, describes an all pass filter, a device that only modifies the signal's phase. We are dealing with the case of $\alpha < 1$, (but generally close to unity) due to losses in the ring: bending, scattering and mismatches between straight and bent modes.

As for the phase,

(2.12) $\theta = n_{eff} \cdot \frac{2\pi}{\lambda} \cdot L = \theta(\lambda, L, n_{eff})$.

L is the geometrical length of the ring (from b_2 to a_2), λ is the vacuum wavelength of the signal and n_{eff} is an effective refractive index of the resonator's WG. For simplicity, the model assumes that this part of the resonator is not affected by the coupling area.

Let us assign the value 1 for the input amplitude a_1, since we deal with the ratio of the other signals to it, and solve for equations **(2.9, 2.11)**. After few algebraic steps, we obtain:

(2.13) $b_1 = \frac{t - \alpha e^{-i\theta}}{1 - t^* \alpha e^{-i\theta}}$, $a_2 = \frac{-\alpha \kappa^* e^{-i\theta}}{1 - t^* \alpha e^{-i\theta}}$.

Thus, the intensity transmission and enhancement in the ring:

(2.14) $T \equiv |b_1|^2 = \frac{\alpha^2 + |t|^2 - 2\alpha|t|\cos(\theta - \phi)}{1 + \alpha^2|t|^2 - 2\alpha|t|\cos(\theta - \phi)}$,

$$Enhancement \equiv |a_2|^2 = \frac{\alpha^2(1 - |t|^2)}{1 + \alpha^2|t|^2 - 2\alpha|t|\cos(\theta - \phi)} \ .$$

Equations **(2.14)** are considered as the main equations of the MRR. One can see that the transmission obtains a minimum at resonance, i.e. $(\theta - \phi)|_{\nu_m} = m \cdot 2\pi$ $(m \in \mathbb{Z})$. This feature of the transmission picture makes the MRR useful for filtering, sensing or

modulation. The power enhancement in the ring obtains a maximum at resonance, and can reach few hundreds if α and $|t|$ are close to unity. In the specific case of $\alpha = |t|$, often called "critical coupling", transmission approaches zero at resonance. We work usually in the case of α slightly larger than $|t|$, known as over coupling.

Few general resonators' characteristics can be obtained, if we plot the transmission against $(\theta - \phi)$: The full width at half maximum [FWHM], is:

(2.15) $\Delta = \frac{2(1-\alpha|t|)}{\sqrt{\alpha|t|}}$.

The normalized Free Spectral Range (FSR) is obviously 2π and thus the finesse is:

(2.16) $F = \frac{FSR}{\Delta} = \frac{\pi\sqrt{\alpha|t|}}{(1-\alpha|t|)}$.

Eventually, the Q factor for the mth resonance is

(2.17) $\mathrm{Q} = \frac{(\theta-\phi)|_{\nu_m}}{\Delta} = \mathrm{mF} = \frac{\mathrm{m}\cdot\pi\sqrt{\alpha|t|}}{(1-\alpha|t|)}$.

We end this section by providing a CMT formula [40] for calculating specific coupling constants. We emphasize that it is a simplified model. For example, in this approach we assume straight WGs in the coupling region. More precise treatment requires taking into account the bending of the ring's WG, as can be found in the relevant literature.

The model uses the separate WGs modes as the Eigen states of the physical problem and assumes the coupling between them to be a small perturbation. An important parameter is the coupling constant, derived from the overlap integral of the modes, which will be marked by ξ. If we define the difference between the two propagation constants to be $\delta = \frac{(\beta_2-\beta_1)}{2}$, a parameter $q = \sqrt{\delta^2 + \xi^2}$ and the coupling region length to be D, it can be shown that equation **(2.9)** gets the form:

(2.18) $b_1 = \left\{\left[\cos(\mathrm{qD}) + i\frac{\delta}{\mathrm{q}}\sin(\mathrm{qD})\right]a_1 - i\frac{\xi}{q}\sin(\mathrm{qD})\,a_2\right\}e^{-i\delta D}$,

$b_2 = \left\{-i\frac{\xi}{q}\sin(\mathrm{qD})\,a_1 + \left[\cos(\mathrm{qD}) - i\frac{\delta}{\mathrm{q}}\sin(\mathrm{qD})\right]a_2\right\}e^{i\delta D}$.

2.3. Short introduction to photonic crystals

A Photonic Crystal (PhC) is a structure which is periodic in its dielectric constant. The PhC can be treated as if the coherent reflections "slow down" the light, and in some cases stop it totally from propagate. This latter case occurs in certain wavelengths or energies that known as "bandgap" or "stop band". This behavior indicates on the resemblance of the PhC to the quantum description of electronic wave function in solid state, where the periodic electrostatic potential influence on the electron's propagation in the same way.

Here we will give short theoretical background of the PhC way of operation, with an emphasis on the slow light concept. We will restrict ourselves to the 1-d case which is the geometry that is studied throughout the thesis.

In a homogeneous medium, i.e. where the dielectric constant ε is constant spatially, the plane EM wave follows a harmonic dependency (for non-dispersive cases):

(2.19) $E(r,t) = E_0 e^{-i[k(\varepsilon)r-\omega t]}$.

The group velocity connects between the wave's spatial and temporal frequencies and is given by:

(2.20) $v = \frac{d\omega}{dk} = \frac{c}{n}$.

Here, n is the medium refractive index which is a direct function of the dielectric constant. One convenient way of presenting a specific mode's velocity is by the use of the dispersion diagram. This is a diagram showing the function $\omega(k)$, which in the homogenous case is nothing but straight lines with a slope that is a function of the medium dielectric constant ε. Such a typical line is shown in Figure 2.3 (red, dashed lines).

However, when a periodic perturbation in ε is generated, i.e. $\varepsilon(r) = \varepsilon(r+d)$, the solution can be shown to have the form:

(2.21) $E(r,t) = u_{m,k}(r) e^{-i(kr-\omega t)}$.

Now, $u_{m,k}(r)$ is a periodic function with the same periodicity d as the dielectric function. The solutions, known as the "Bloch modes", can be plotted in a dispersion diagram, where it is sufficient to plot the region of $|k| \le \frac{\pi}{d}$ (known as the first Brillouin zone) due to the structure's symmetry. A typical dispersion curve is shown in Figure 2.3.

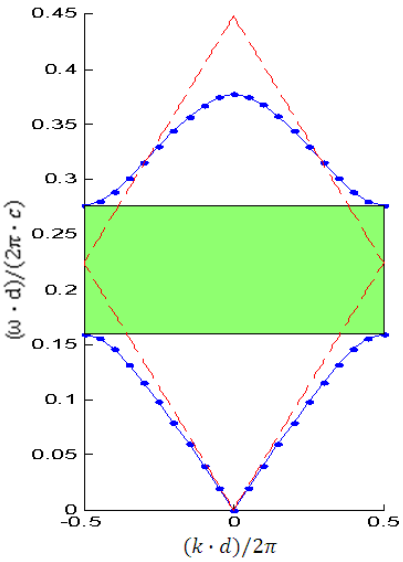

Figure 2.3: A typical dispersion diagram. Plotted is a dispersion diagram for the case of a multilayer film consists of alternating layers of Silicon and air, with width of d/2 each. The dashed lines are the light lines for the case of homogenous bulk with an averaged refractive index. The green area represents the stop band. The picture was simulated by Mr. Boris Desiatov from the nano-opto group, and appears here with his kind permission.

One can easily notice that stop bands can appear. In the scope of this thesis we focus on the region near the band edge, where the light can still propagate along the structure, but the slope of the dispersion line gets very close to zero. In other words, the light experiences the physical effect of **slow light**, where the group velocity tends to zero (while the group index, which is the ratio between the light vacuum velocity to the group velocity of the wave, tends to infinity).

3. Analytical approach

We begin by developing an analytical model based on a CMT approach to calculate the GOF. For simplicity, we consider a 2-dimensional rather than a 3-dimensional structure. The validity of this assumption will be discussed later, in the numerical chapter. Nevertheless, in its essence the analytical model is completely general and few small changes should be made to transform it to a 3-d model.

A schematic diagram showing our model is presented in Figure 3.1(a). To simplify the problem we consider a symmetric coupling region having its mirror symmetry in the middle of the coupling region, as shown in Figure 3.1(b). The system is excited by an EM wave of time-dependency $e^{i\omega t}$, and all the WGs are assumed to support a single mode.

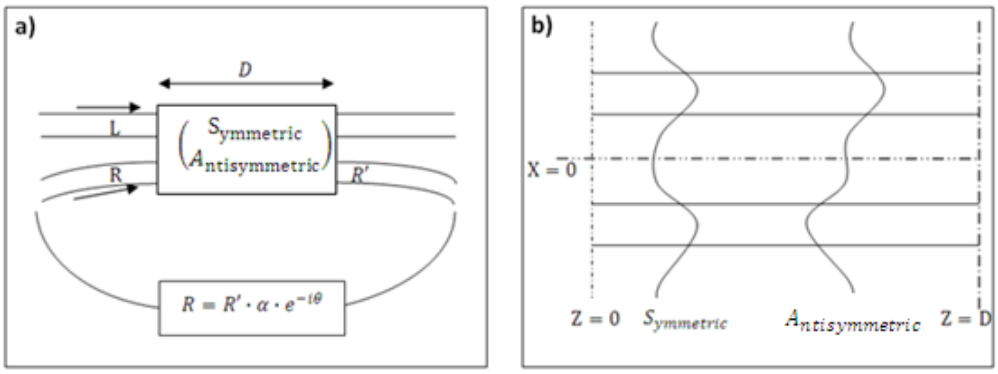

Figure 3.1: Schematics of the 2-d system. (a) The notations of the EM fields in the bus WG and in the MRR as well as the phase accumulation in the MRR are shown. (b) The coupling region is sketched together with the two supermodes.

The time-averaged GOF acting on the bus WG along the x-axis is calculated via the MST. For our structure and for a given polarization, e.g. the Transverse Electric – TE (the treatment for the Transverse Magnetic – TM polarization is obviously equivalent), the complicated definition of equation **(2.4)** is reduced to [5,8]:

(3.1) $$F_x = \frac{1}{4}\cdot[-\varepsilon_0 \left|E_y\right|^2 + \mu_0(\left|H_x\right|^2 - \left|H_z\right|^2)] .$$

This component is actually in units of pressure, i.e. force per area. No integration of the MST component on the y and z axes is performed since it is invariant in these two directions: it is infinite along the y axis and it has a translational symmetry along the propagation direction, i.e. the z axis (as long as we deal only with the coupling region). We assume a coupling region in which the gap between the two WGs is kept constant. This geometry maintains its mirror symmetry which allows the decomposition of the incident EM field into symmetric (S) and anti-symmetric (A) modes. These are the eigenmodes of the coupling region.

Following previous work [10] one can express the incident field at the coupling region by

(3.2) $$\psi = L + R .$$

Where ψ stands for the magnetic or electric field component, while L and R are the incident fields at each of the bus WGs. Generally, L and R can be arbitrarily chosen. However, in the case of an MRR, R is replaced by $R' = w \cdot R$ where R is identical to L both in its amplitude and its phase and w is the complex ratio between the field in the MRR and the incident field (in fact it is a_2 of Equation **(2.13)**). Using sec. 2.2 we can write:

(3.3) $$w = \frac{-i\alpha \cdot e^{-i\theta}\sin(\kappa \cdot D)}{1-\alpha \cdot e^{-i\theta}\cos(\kappa \cdot D)} .$$

Here, α and θ are the field amplitude fraction remaining after a roundtrip in the ring and the phase accumulated in the resonator roundtrip, respectively. D is the coupling region's length, and κ is the coupling coefficient between the WGs. Therefore, equation **(3.2)** takes the modified form of:

(3.4) $$\psi = L + w \cdot R .$$

At $z = 0$ we express the fields in each WG as a superposition of symmetric and anti-symmetric modes:

(3.5) $$\begin{pmatrix} L \\ R \end{pmatrix} = \begin{pmatrix} a & b \\ c & d \end{pmatrix} \begin{pmatrix} S \\ A \end{pmatrix}.$$

Where,

(3.6) $$a = \int L \cdot S^* dx = \int R \cdot S^* dx = c, b = \int L \cdot A^* dx = -\int R \cdot A^* dx = -d \ .$$

Substituting Equation **(3.4)**, **(3.5)** and **(3.6)** in Equation **(3.1)**, the GOF acting on the bus WG can be written as:

(3.7) $$\begin{aligned} F = {} & a^2(1+|w|^2 + 2\Re\{w\}) \cdot F_{sym} + b^2(1+|w|^2 - 2\Re\{w\}) \cdot F_{antisym} \\ & +2ab\Re\{e^{-i\cdot\Delta\beta\cdot z}(1-|w|^2 + 2i\cdot\Im\{w\})\} \cdot F_{\text{int}erference} \end{aligned} .$$

Here, F_{sym} and $F_{antisym}$ are the forces calculated for each of the two supermodes supported by two WGs system, $F_{\text{int}erference}$ is calculated by taking the product of the symmetric and anti-symmetric field for every squared field component, $\Delta\beta = \beta_{symmetric} - \beta_{antisymmetric}$ is the difference between the propagation constants of the two supermodes, and z is the propagation length in the coupled region. Clearly, the third term in this equation oscillates with the propagation coordinate (z).For the purpose of calculating the GOF (per unit length) acting on the WG we can simplify this term by taking its averaged value. This simplification is justified for large gaps between the WGs, due to two reasons: 1- $\Delta\beta$ is relatively small, so averaging is legitimate. 2- As was already shown [10], the contribution from the beating term is negligible compared to the symmetric and anti-symmetric GOF terms, because of the small overlap integral of the symmetric and anti-symmetric modes.

Thus, the recipe for calculating the GOF following equation **(3.7)** is taking the EM modes of the double WGs system and calculating the corresponding force components. Afterwards one needs to calculate equations **(3.6)** using the EM modes of the single WG. Finally, the parameters of the ring and the coupling region are introduced.

It is important to emphasize that the qualitative behavior of the force in the vicinity of resonance arises from the general analytical model. Thus, different parameters lead all to the same behavior. Figure 3.2 shows the force as a function of

wavelength as calculated from equation **(3.7)** for a specific 2-D MRR system, together with the MRR power enhancement spectrum.

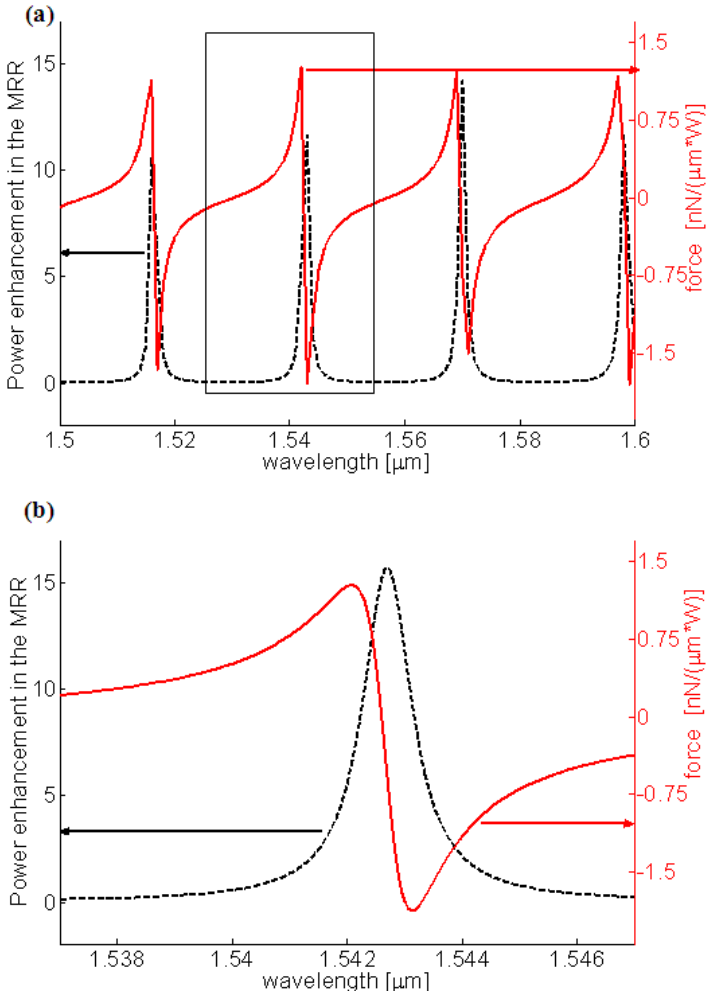

Figure 2.2: (a) Power enhancement and GOF as a function of wavelength. A 250nm gap is assumed between two 400nm slab WGs with $n = 2.446$. The WGs are coupled along a coupling region of $4\mu m$. The MRR properties are provided in the numerical section. (b) Zoom in on the region denoted by the rectangle.

From first glance, the results are surprising- the largest GOF is not obtained at resonance, where the field enhancement is maximal, but rather at two extreme values, with opposing sign, occurring slightly before and after the resonance peak. These extreme values are indeed large compared to the force obtained in an equivalent two slabs system. However, the enhancement factor is in the order of 2-3, corresponding to the MRR power enhancement at these wavelengths which are slightly off resonance.

This counter-intuitive behavior of the force has been experimentally observed in a disk resonator system [30], and the results were explained by a quantum theoretical model. We next use our CMT-based model to explain this finding.

It has been shown [10] that the GOF depends dramatically on the relative phase between the fields in two adjacent WGs. This relative phase controls the excitation of each of the eigenmodes in the system, and consequently the ratio between the attractive and repulsive components of the force. In other words, the GOF is not only a function of the fields' amplitudes but also a function of their relative phase.

We now go back to equation **(3.7)** and focus on the region of interest near resonance, where the amplitude of w tends towards its maximum. As appears from equation **(3.3)**, at resonance one obtains $\Re(w)=0$, meaning that the relative phase between each component of the EM field in the bus WG and the MRR is $3\pi/2$. At typical gap separation, each of the coefficients of equation **(3.6)** approach the value of $1/2$, and thus at resonance equation **(3.7)** can be expressed as:

(3.8) $$F\left|_{resonance}\cong\frac{1}{4}(1+\left|w\right|^2)\cdot[F_{sym}+F_{asym}]\right..$$

As was previously shown [4,5,8,23], at large enough separation gaps the symmetric force is attractive (negative sign in our conventions) whereas the anti-symmetric force is repulsive (positive sign). Thus, although the field enhancement is maximal, the opposing sign of the two force components will reduce the total net GOF. On the other hand, if the relative phase tends towards 0 or π, while the system is still in the vicinity of resonance (in order to have a significant field in the MRR), maximal attractive or repulsive force will be obtained, respectively.

4. Numerical simulations

While the analytical model supports the physical understanding of the parameters affecting the force in the system, it cannot be fully correlated to an actual structure. Therefore, numerical simulations are needed for quantitative design and analysis of the forces in the MRR system. Moreover, the numerical simulations allow coping with more complex structures, e.g. asymmetric structures. These will be shown to play an important role in our work. Throughout the paper, the numerical calculations are performed by the Finite Element Method (FEM) using COMSOL software. This chapter is devoted to the EM numerical simulations.

4.1. The system design

For the numerical simulations, we need to determine the exact system's geometry and the operation conditions. Our guiding lines for choosing the proper system are achieving the largest possible force values while keeping in mind that fabrication considerations should be taken into account.

4.1.1 Cross-sectional area simulations

First, we investigate the double rectangular WG system, separated in the horizontal dimension, as detailed for example in [4]. This structure has translation symmetry in the propagation direction, so the computation dimensions can be reduced to two-dimensional calculations on the cross section of the two WGs. Figure 4.1 illustrates the geometry and the axes used in our work.

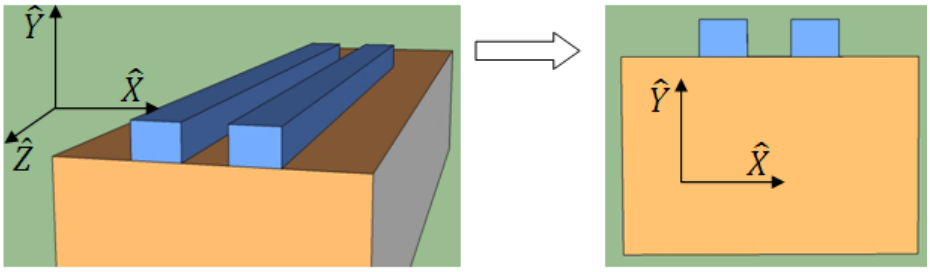

Figure 4.1: schematic drawing of the 2 WG structure. The full-structure picture on the left has translation symmetry so the calculations on the cross section (shown on the right), are sufficient. The axes for the geometry are presented as well.

First, we extract the EM eigenmodes of the WGs, and then calculate the force values (per injected intensity unit) by integrating the relevant MST component on the 4 edges.

As a background, one should be familiar with such a structure. We deal with (almost) single-mode WGs, i.e. for each polarization a single WG has only one mode. For the doubled system the symmetry gives rise to mode splitting. We obtain eventually 4 modes: symmetric and anti-symmetric (referring to the mirror axis between the two WGs, i.e. $\hat{X} = 0$) for each of the two polarizations. Full description of such a system can be found in [4] or elsewhere. For clarity, We plot here (Figure 4.2) these 4 modes for the case of Silicon ($n = 3.45$) WGs, with cross sectional dimensions of $500 \times 250\ nm^2$, at the telecom vacuum wavelength of $\lambda = 1550nm$. For these dimensions, the In-Plane (INP) polarized modes (i.e. dominant electric field is directed along the x axis) are much more confined than the Out-Of-Plane (OOP) ones (i.e. dominant electric field is directed along the y axis). When the WG becomes more squared, this property is weakened.

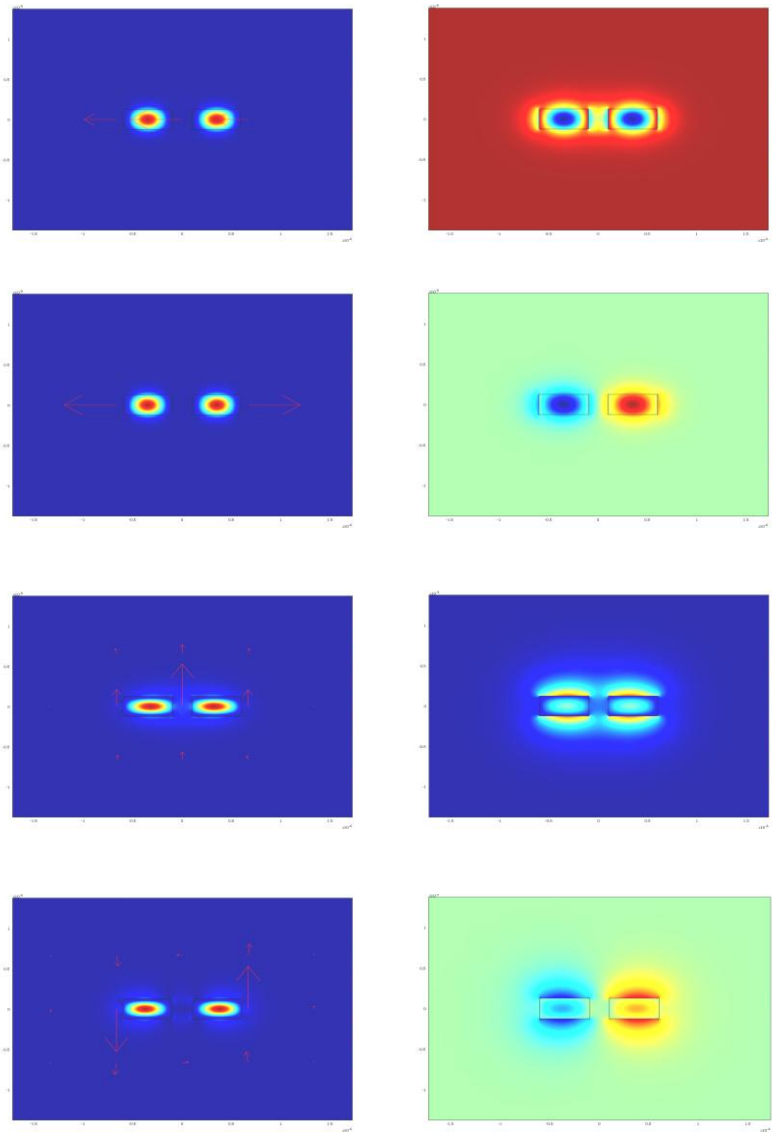

Figure 4.2: the 4 modes of the double rectangular WG. The left figures are the Poynting Vector distribution, while red arrows are superimposed to mark the electric field's direction and magnitude. On the right figures, the corresponding dominant electric field distribution is plotted. The modes order is from the most confined mode (top) to the least one (bottom). For visualization purposes the color scale between the figures is modified.

We are now at a position to select the parameters. These include the WGs dimensions and refractive index and the operation signal's wavelength and polarization.

As for the WG dimensions, [4] operated with relatively small cross sectional dimension of $310 \times 310\, nm^2$. As we will see, this enlarges the force, but due to fabrication considerations we prefer to design a device with dimensions that were

previously fabricated in our lab, i.e. $500 \times 250\, nm^2$. We examine the main GOF component (the x component) at these two parameters sets and also at an intermediate value of $400 \times 300\, nm^2$, for constant wavelength and constant material, for the two available polarizations. The obtained GOF is presented in Figure 4.3 against the separation gap.

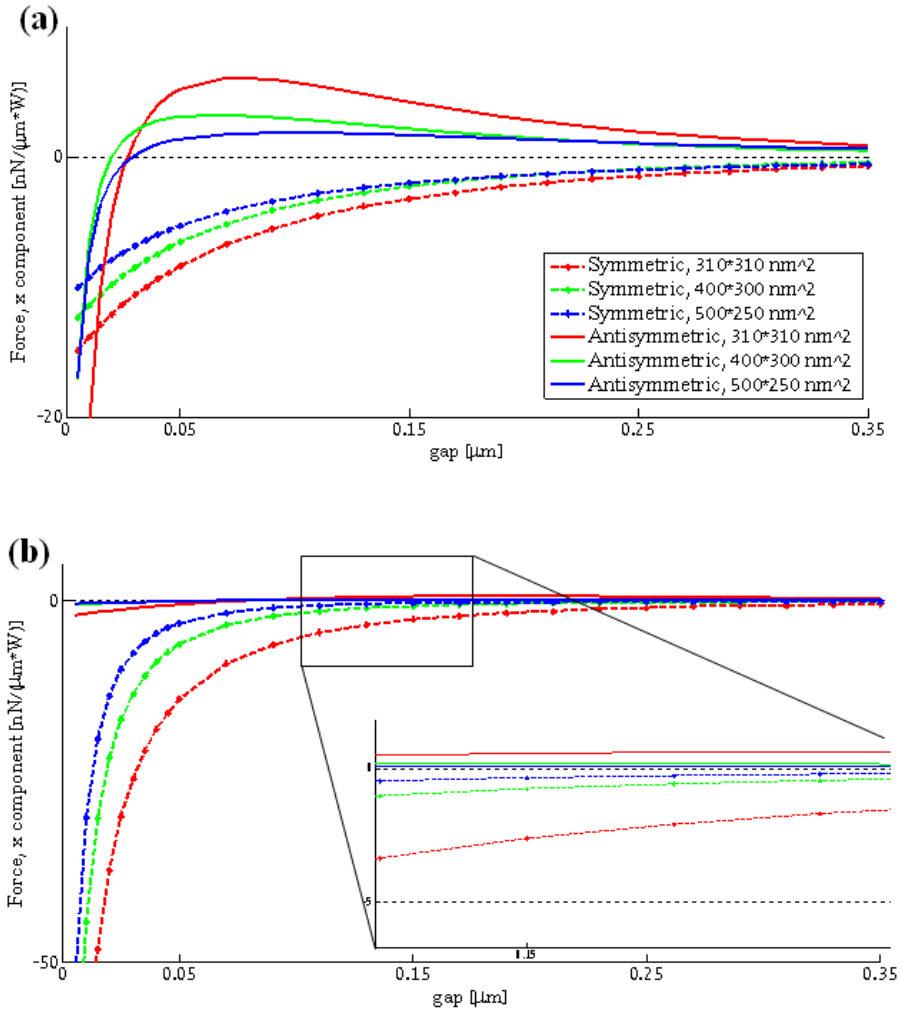

Figure 4.3: gap dependence of the GOF and the dimensions' effect. The gap between the WGs is changed and the force is calculated for 3 different WG dimensions. (a) The force for the two modes for OOP polarization illumination. (b) The same, for INP polarization illumination. The region marked in rectangle is zoomed in the inset.

As appears in the figure, the basic behavior of the force is similar at all sizes and polarizations- the symmetric mode produces negative force, decreasing with the increase in separation gap. The anti-symmetric mode produces a positive force which

is reduced with the increase in separation gap. However, for small gaps the anti-symmetric mode's force changes trend and even its sign and can become even more attractive than the force of the symmetric mode. These global features are well known in the literature [4,5,8,23], and their investigation is beyond the scope of our work, although we can state in general that it has to do with the behavior of the electric field at the edges. As for our work, we focus on relatively large gaps (above 150 nm) due to the fact that in the MRR system large gaps are needed for small coupling and reasonable Q factor.

Referring to the two possible polarizations, it seems that the INP polarization can give rise to higher force values compared with the OOP polarization. This is true if we work with the symmetric mode and at very small gaps. However, as we stated, we need to work in the larger gaps regime, and thus after carefully examining the force values we concluded that in our case the attractive force is about an order of magnitude smaller than its correspondent generated by the OOP polarized mode. Considering that, we will focus on the later (which is also referred as TM-like), as also [4] and other works have done.

Examining the effect of the WG sizes on the GOF, it is easy to see that shrinking the structure will lead to better results (although not dramatically). This feature is expected, and can be explained by the fact that the force is based on the field change due to the presence of the second WG. As such, the lower mode confinement results in higher mutual influence between the WGs and the force will be increased [11]. This also explains why at large enough gaps (where edges effects do not exist) the more confined modes of the INP polarization generate lower force. Anyway, since we deal with large gaps, and the differences between different WG sizes are not enormous, we will limit our discussion to cross sectional dimensions of $400 \times 300\ nm^2$, in order to simulate more realistic device.

Figure 4.4 is devoted to examine the frequency influence and the refractive indices' difference effect. For this latter parameter, we set the WG's core to be Silicon and check the cladding's index. We fix the separation gap to 200nm and work with the dimensions and polarization chosen before. We also take into account the dispersion of Silicon in such a broad wavelength regime.

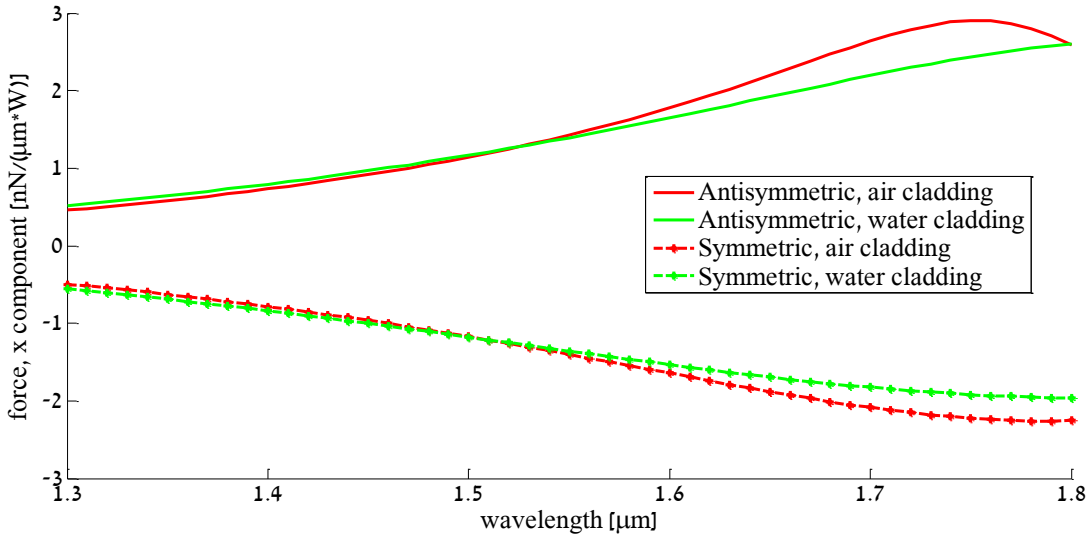

Figure 4.4: spectral dependence of the force and cladding influence. The examined structure consists of two $\mathbf{400 \times 300\ nm^2}$ Si WG, with 200nm separation gap, under OOP polarization illumination.

Generally, the force grows moderately with wavelength, which has also been explained [11] by the simple fact of decrease in the level of mode confinement (the slight decrease at large wavelengths is also explained there). We aim to operate at telecom wavelength (which is the typical choice for Silicon photonics), where the relative change in force as a function of wavelength is quite small. In addition, in this spectral region no dramatic change is observed by changing the cladding from air to water ($n = 1.33$), for example.

It is worth mentioning that a lot of works use Si3N4 as the WGs material. This enables slightly larger forces and much more injected intensity (to obtain significant effects), but on the other hand the MRR should be much larger to avoid significant bending losses. For the scope of this thesis, we limit ourselves to the Silicon.

Concluding this part, our basic WG consists of a Silicon core surrounded by air (in some of the cases it will partly lie on SiO_2 substrate). Its dimensions are chosen to be $400 \times 300\ \text{nm}^2$. Referring to the illumination, we operate at wavelength around $\lambda = 1550nm$, and the polarization is OOP (major electric field is directed along the y-axis).

4.1.2 Ring resonator parameters

After selecting the basic WGs structure, the ring's design should be considered. The separation gap between the ring and the bus WG will be discussed later in the thesis.

Taking advantage of the large index ratio between core and cladding in silicon WGs, which manifests in small bending loss even for small radius, we chose the MRR radius to be $5.13\ \mu m$.

Another degree of freedom is the specific ring geometry. Several works were based on a "racetrack" structure, i.e. a ring with two additional straight WG sections (see the schematic Figure 1.2). Its main feature is enlarging the coupling area of the ring and the bus WG. We will use this kind of structure in some cases. Additional losses are introduced in these structures because of the mode-mismatch between the straight WG mode and the bent WG mode. The losses that eventually present in a structure that includes two $2.67\mu m$ straight WG sections have been calculated to be $0.0113\frac{dB}{roundtrip}$. Different aspects of the racetrack shape will be discussed afterward.

4.2. The two-dimensional approximation

Before moving to the actual simulations, a major approximation should be done. Performing FEM calculations on a system of an MRR coupled to a bus WG is numerically intensive. Therefore, we considered the simplification of our geometry by the use of the Effective Index Method (EIM) allowing obtaining a 2-D geometry (we eliminate the height of the structure, i.e. the dimension in which the whole system is a simple single mode WG). The validity of the method was intensively explored and discussed, for example in [40,41]. It was also used in an MRR analysis, for example in [42]. One should keep in mind that the actual resonance frequencies and the quality factors may be slightly different in real (3-D) geometry. However, we expect the qualitative behavior and the orders of magnitude to be predicted by the 2-D approximation.

Let us explain first the principle of the EIM. For our case of rectangular WGs, the method is quite simple and works as follows: the dimension to be neglected is scanned so the WGs considered as slabs, 300nm width, $n = 3.45$, top cladding of $n = 1$ and substrate of $n = 1$ or $n = 1.46$ for the case of the air bridged WG or the standard one, respectively. After setting the polarization to TM (see figure 4.5) and calculating for the specific wavelength one gets the propagation constant, and consequently the effective index of this slab's mode. This effective index is to be taken as the new core index. We now considering a system of "slab" MRR, 400nm width excited by TE polarized light.

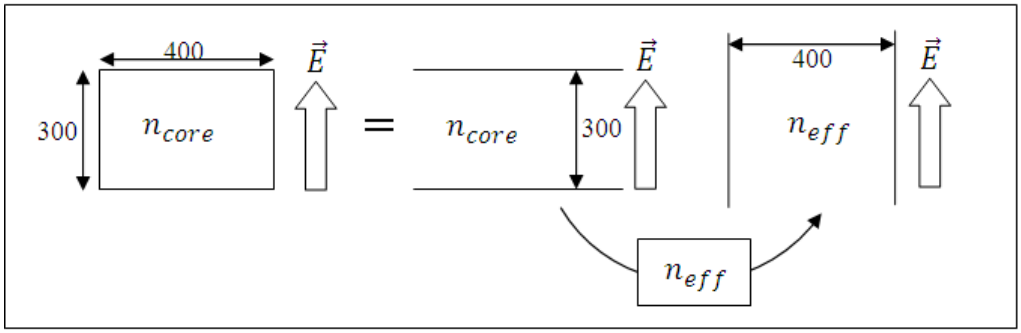

Figure 4.5: the Effective Index Method in the rectangular WG. The rectangular WG on the left is investigated via applying two consequent slabs treatment: the first one is using one of the dimensions and the real core's index and produces an effective index. The second treatment analyses the other dimension using the effective index produced in the first treatment as the core's index. The polarization of the incident light is constant, so in the different treatments it will be treated differently.

Specifically, by this method we get $n_{eff} = 2.446$ for the Silicon-on-air WG, and $n_{eff} = 2.525$ for the Silicon-on-SiO_2 one.

Nevertheless, besides the photonic behavior, the dimension reduction has an influence on the forces calculation, mainly because of edge effects on the y direction which do not exist in the 2-D version. Therefore, the legitimacy of the use of the 2-D approximation needs to be checked. To validate this approach, we use a simplified system of two optical WGs and compare the obtained force in two cases: full 3-dimensional system and an approximated system with the EIM (effectively two slabs). We first consider a structure of two WGs (with the same parameters discussed

already) which are separated along the horizontal direction. In Figure 4.6 the calculated GOF component is plotted against the separation gap (blue lines). Next, we calculate the GOF for the same system using the effective index approach, where the y- dimension was eliminated, by replacing the air-300 nm silicon-air structure with a single infinite layer having an effective refractive index of 2.446. The calculated forces are also plotted in Figure 4.6 (red lines). This latter 2-D treatment is by FEM propagation picture since this is the frame in which the full simulations are made, although in this case of 2 slabs an analytical procedure is also available [1,8] , which gives almost identical results.

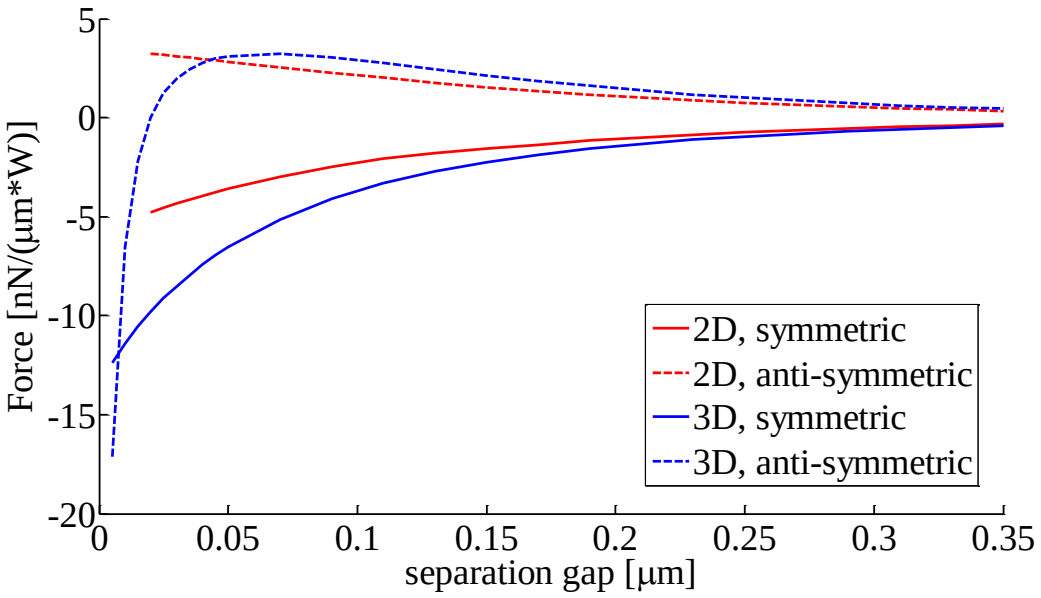

Figure 4.6: The GOF calculated for two Si (n=3.45) WGs having identical cross sections of $400 \times 300\ \mathrm{nm}^2$. The WGs are excited by an out of plane (TM) polarized, laser source at the wavelength of $\lambda = 1550\mathrm{nm}$. The broken lines (solid lines) represent the force for an anti-symmetric (symmetric) mode excitation. The blue lines are the full three dimensional calculation, while the red lines refer to a two dimensional system, effectively two slabs of 400nm with n=2.446.

As can be seen, the behavior in small gaps is certainly different for a strip WG or for a slab, apparently due to the electric contribution to the EM force which is related to edge effects. Nevertheless, for gaps larger than approx. 150nm we get almost identical numbers, and the slight difference can be attributed to the difference in the meshing between the two cases. We conclude that the effective index approximation is sufficient for our purposes as long as we remain on the large gap

regime, which is the scenario of this work because of the low-coupling-loss needed in the MRR, and in particular if operating with racetrack structures.

As a comment, it should be mentioned that by this 2-D approximation the values of the fields, intensities and forces will be per unit length. Generally we will be interested in the force obtained as a result of specific intensity injection, so the force per unit length will be divided by the intensity by unit length and the unit mismatch is cancelled out. However, converting to real intensity that is launched into the WG requires normalization. One can show by accurate calculations (which can be also supported by logical argument) that the procedure for obtaining real intensity value is multiplying the intensity per unit length by an effective height which is equal to half of the actual WG height.

4.3. Averaging of the force

Clearly, the force distribution along the bus WG is not constant due to the variation in the coupling to the MRR throughout the light propagation. However, the standard notation in the scientific community and also the equations of the mechanical response of the WG make use of force per unit length (in the propagation direction). Consequently, the force values in this paper are given in force per unit length, after averaging along the bus WG, by integrating the force along the WG's length and then dividing by the integration length. To validate this method we perform the following procedure. Three different force distributions are simulated, which represent three cases: 1 - a ring structure and 2 - a racetrack structure (having two additional $2.67\mu m$ long straight WG sections) which have the same average value and 3 - a hypothetical rectangular force distribution which represents our method, meaning constant value (of the same averaged number) along certain length. These distributions are shown in Figure 4.7(a). The exact conditions for obtaining these force distribution values, in the case of a ring resonator (which requires smaller separation gap) and a racetrack resonator (larger separation gap) are not critical at this point.

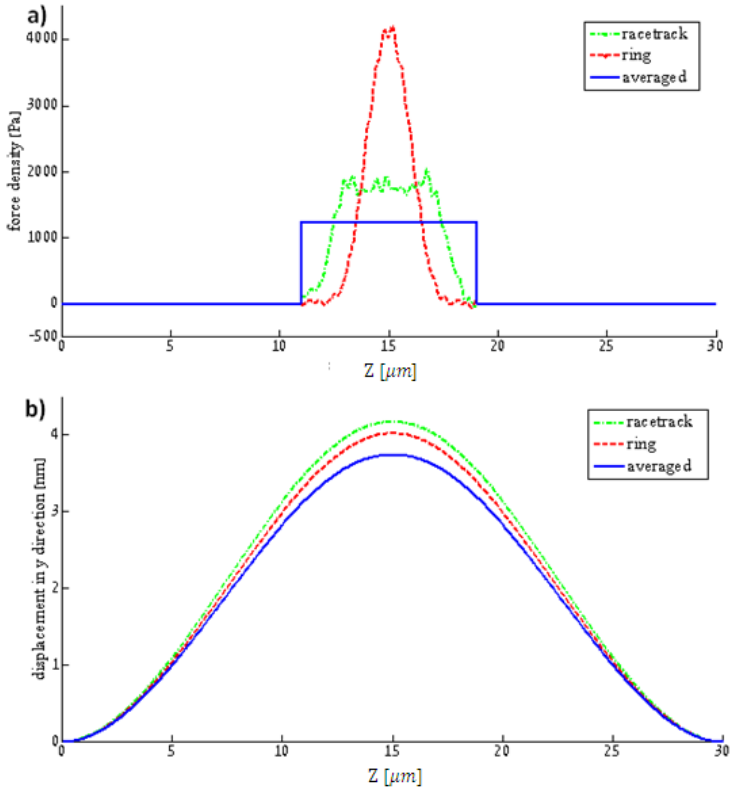

Figure 4.7: Force averaging in the propagation direction. The force density distribution for two equivalent structures in terms of average force, are presented in (a): ring and racetrack MRRs (with two different gaps). The averaged rectangular force is plotted as well. The mechanical response of the $30\mu m$ air bridge WG is plotted in (b) for these 3 cases.

Next we simulate the mechanical response of a 30 μm-free bus WG as a result of these force distributions, taking into account the Si elastic properties (as will be explained in sec. 4.5). The results are shown in Figure 4.7(b). As can be noticed, only a slight difference (few percentages) is obtained when an averaged force is present. This fact supports our method of calculation. In other words, as long as displacement is the parameter of interest, the bus WG feels the force as if acting on its center of mass regardless of the exact force distribution.

Additionally, these simulations prove that no fundamental difference exists between a ring and a racetrack structure as long as the net integral of the force is equal. This is in contrast to our naive assumption that the GOF obtained in a racetrack structure will generate an enhanced effect due to its larger coupling area. Indeed, for a

specific gap the ring's effective area is smaller but the Q factor is higher, so the total force's effect remains unchanged.

4.4. The electromagnetic simulations

We first use the numerical simulation in order to validate the results of the analytical model. Indeed, the force obtained with the numerical calculation is very similar to that calculated by the analytical model. Two typical plots, amongst lots of simulations, are presented in Figure 4.8:

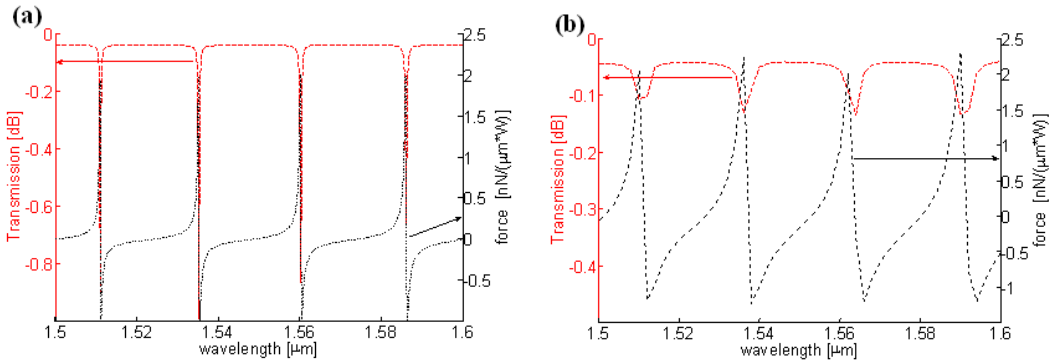

Figure 4.8: Numerical simulations of the GOF and the transmission of light as a function of the wavelength. (a) The refractive index of both the MRR and the bus WG is n=2.446, the separation gap is 350nm and the extension of the racetrack is 2.67 μm long. (b) The refractive index of both the MRR and the bus WG is n=2.52, the separation gap is 150nm and the extension of the racetrack is 1 μm.

The numerical simulations allow us to extract additional information compare with the analytic model. In Figure 4.9 we present the electric field distribution in the coupling region at resonance and at adjacent wavelengths for which the force approaches its extreme values. As was predicted by the analytical model, the maximal repulsive (attractive) force is obtained when the relative phase between the fields in the WG and the MRR is close to $\pi(0)$, while at resonance the $3\pi/2$ phase difference at the beginning of the coupling region reduces the net force.

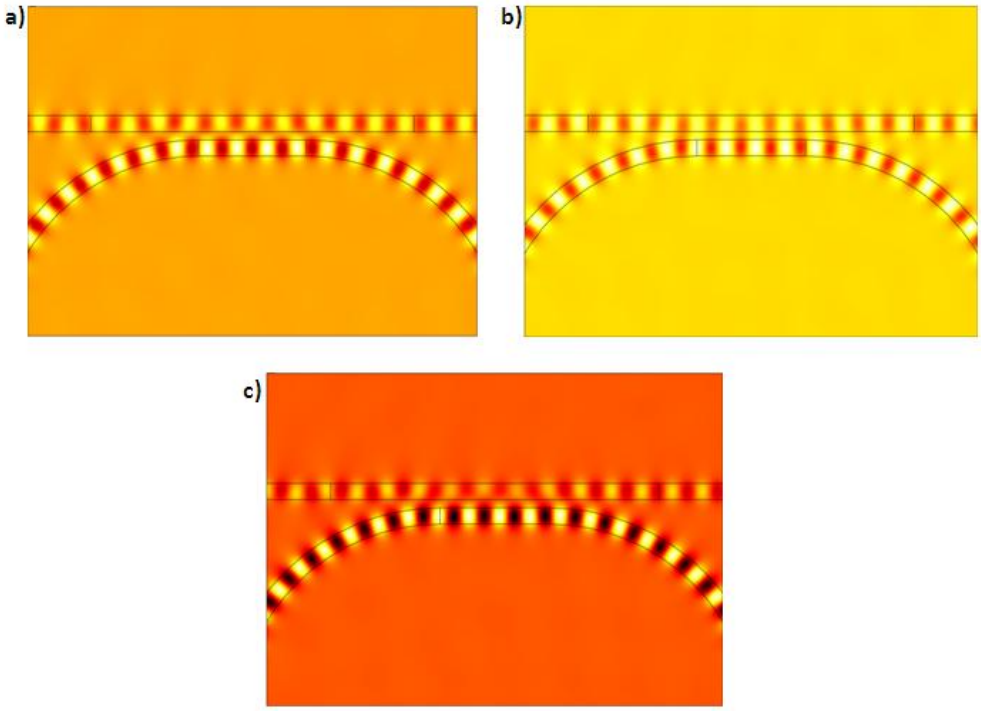

Figure 4.9: The electric field distribution in the coupling region of the racetrack MRR is shown. Figure (a) [(b)] were calculated at wavelength in which the obtained force is maximal positive [negative], where the relative phase between the signals is close to π [0]. Figure (c) was calculated at a resonance wavelength in which the relative phase at the beginning of the coupling region is $3\pi/2$. The phase difference evolves and becomes $\pi/2$ at the output of the coupling region. For visualization purposes we modified the color scale between the 3 figures.

In order to maximize the GOF, it is desired to operate at resonance, where the power enhancement is maximal. At the same time we wish to operate at phase matching condition, i.e. to have a relative phase between the bus WG and the MRR approaching 0 or π, giving rise to the dominancy of either the symmetric or the anti-symmetric force term.

To do so, we introduce an a-symmetry to the structure (by modifying the parameters of one of the WGs). We can use the CMT to show that indeed this procedure generates the desired result. If we take equation **(2.18)** that introduces difference between the coupled WGs and plug it into equation **(2.13)**, the coefficient w becomes of the form:

(4.1) $$w = \frac{-i\cdot\alpha\cdot\frac{\xi}{q}\cdot\sin(\mathrm{qD})\cdot e^{i(\delta D-\theta)}}{1-\alpha\cdot[\cos(\mathrm{qD})-i\frac{\delta}{\mathrm{q}}\sin(\mathrm{qD})]\cdot e^{i(\delta D-\theta)}}$$

We notice that in the case of resonance ($\theta = 2\pi \cdot m$) the relative phase deviates generally from $3\pi/2$, and in some cases it can even approach 0 or π.

From now on through the thesis we do not use the analytical model developed in chapter 3, since few of its assumptions do not hold anymore (e.g. the decomposition to symmetric and anti-symmetric modes, the correctness of equation **(3.6)**). If so, we proceed with the numerical calculations.

The first step towards creating the needed asymmetry is by allowing the bus WG to be in a free standing configuration, whereas the MRR is assumed to be positioned on top of a SiO_2 substrate. This geometry supports the required mechanical translation of the bus WG and at the same time is preferable for the obtaining of a stable MRR with a high Q factor. In this configuration, the effective refractive index of the MRR and the bus WG are 2.52 and 2.446 respectively. However, from numerical calculations we conclude that this slight difference in effective indices is not sufficient, and the MRR's effective refractive index should be $n_{eff} = 2.66$, i.e. effective index difference of nearly 0.22. This can be achieved e.g. by increasing the height of the MRR from 300nm to 325nm (based on EIM calculation). Alternatively, we can choose a wider MRR WG. The latter is preferable from fabrication point of view.

This calculated n_{eff} depends up to some extent on the exact shape of the MRR, and the given number is accurate for a racetrack structure with two $2.67\,\mu m$ long straight WG sections. Interestingly, we succeed in applying the method only to the racetrack structures and not to the ring structure. This may be the result of non sufficient propagation length in the coupling region.

We now repeat the numerical simulations with an MRR effective index value of 2.66. The obtained power enhancement and force as a function of wavelength in the vicinity of a single resonance are presented in Figure 4.10, where the force and the power enhancement curves are nearly consolidating, and the force obtains its maximum absolute value around the wavelength of resonance, where the power enhancement is maximal.

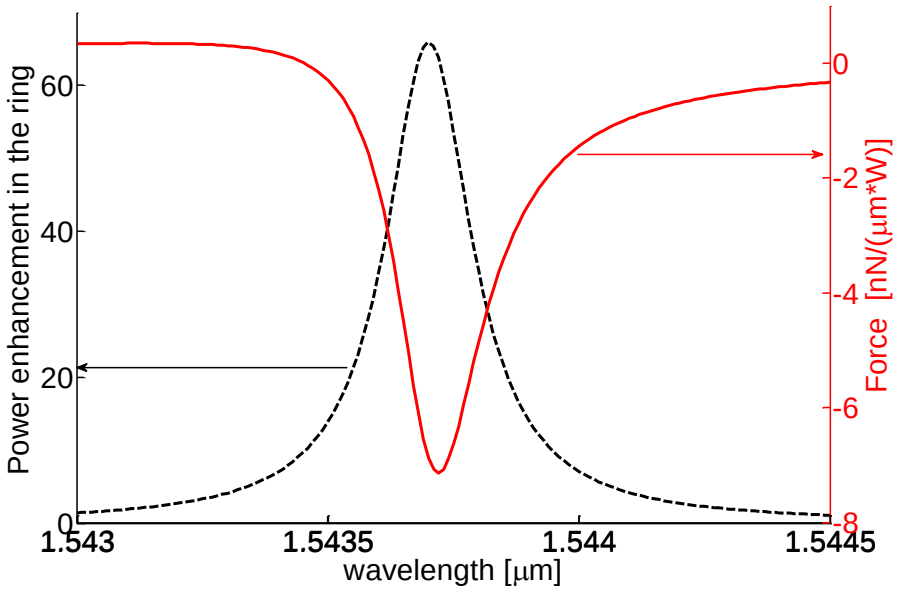

Figure 4.10: The force in an asymmetric MRR system against wavelength. The effective refractive index of the MRR is assumed to be 2.66. The separation gap is 250nm. These parameters corresponds to quality factor of $Q \cong 10{,}000$.

With this improvement we can now investigate the obtained force values and their relation to the MRR power enhancement. In Figure 4.11 we sketch the force as a function of wavelength for numerous separation gaps between the MRR and the bus WG. First, we notice the narrowing of the force curve as the gap separation increases. This is expected because the coupling between the bus WG and the MRR is decreasing, effectively increasing the Q factor of the MRR. The narrow force curve will be used in the next section, where we discuss the tunability of the optical system using optical forces. In addition, we notice an increase in the force at resonance with the decrease in the gap separation. Here we need to take into account two phenomena with opposite effect on the force. On one hand, by reducing the separation between two WGs, one expects the force to increase as a result of stronger interaction. On the other hand, the resonant enhancement of the force becomes less prominent, due to the decrease in Q factor. We now focus on this latter effect by comparing the force at resonance to the force obtained in a double WG system with the same separation gap. The result is shown in the inset of Figure 4.11.

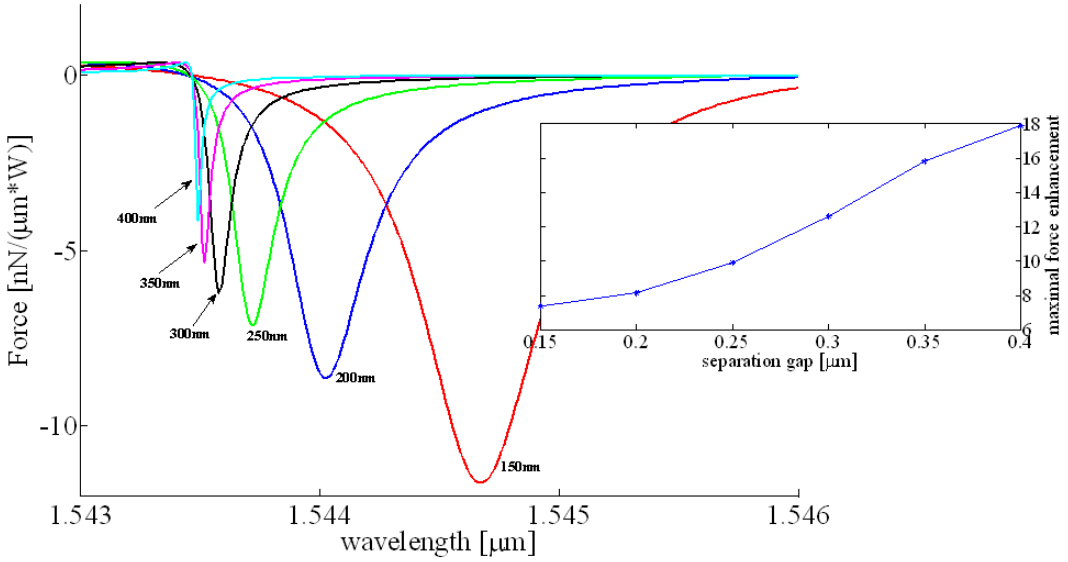

Figure 4.11: Force as a function of wavelength for different gaps between the bus and the MRR. As can be seen, the Q factor grows with the increase of the separation gap. However, the magnitude of the force decreases with the increase in separation gap, because of the lower overlap between the mode and the WG. The inset shows the maximal force values normalized by the force that is obtained in the 2 slabs system for the same gap, as a function of the separation gap.

Indeed, we notice an increase in the force enhancement, following the improvement in the Q factor of the MRR. However, this enhancement is not following the power enhancement in the MRR. This feature can be explained by the fact that the optical power is only enhanced in the MRR, but not in the bus WG. The exact amount of enhancement can be estimated by CMT and it depends generally both on the MRR enhancement and on the exponential decay of the MRR WG mode.

4.5. Mechanical simulations

In order to estimate the coupled opto-mechanical effect, we combine the EM simulations together with structural simulations to predict the translation of the bus WG as a result of the GOF. We assume a separation gap of 250nm (see Figure 4.10), for which the obtained quality factor and maximal force are $Q \cong 10,000$ and $F_{\max} \cong 7[nN/(\mu m \cdot W)]$ respectively. We assume the section of the air bridged WG, i.e. the free standing beam to be $28\mu m$ long. For the Silicon's elastic parameters we use known data from the literature. As an example, if we decouple the EM and the

mechanical simulations (i.e. the GOF for the specific parameters is obtained and then serves as the data for a mechanical simulation), the parameters will result in maximal beam deflection of 5.6nm for an incident power of 50mW in the bus WG. Figure 4.12 presents this situation schematically.

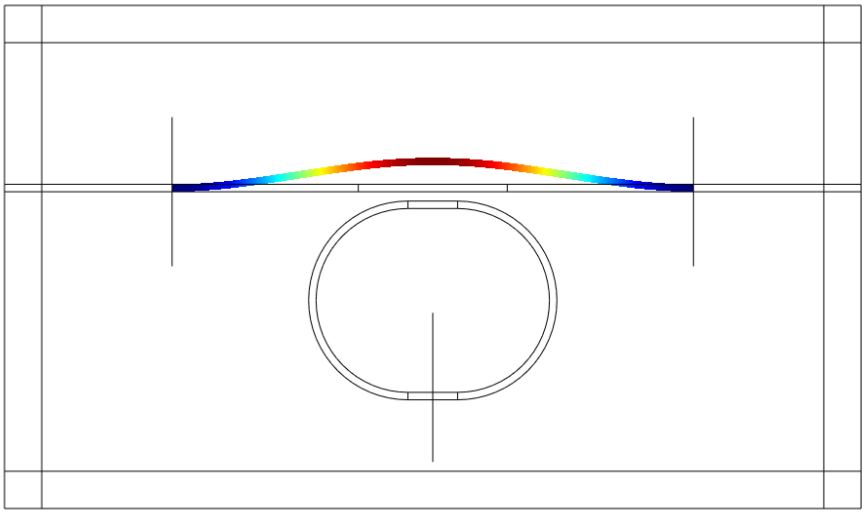

Figure 4.12: The deflection of the beam as a result of the GOF. The geometry that serves for the elastic simulations is shown, where the whole structure is set to be fixed accept for 28 μm long bus WG section which is free to move. The force per unit length is implemented on a region of about 8 μm. The deflection shown in the picture is about 300 times enlarged compared to the actual displacement.

While the latter value provides an estimate for the strength of the effect, a more rigorous analysis which takes into account the mutual effect of the EM fields and the geometry of the device is needed. For example, a shift in the device geometry may result in a transition of the MRR out of resonance. This in turn will reduce the strength of the EM field in the resonator. As a consequence, the beam will tend towards its original geometry, and the process will repeat itself.

In Figure 4.13 we show explicitly the combined opto-mechanical effect. We compare between low (1mW) and higher incident power (25mW) feeding the device. For the latter, the wavelength of maximum power in the MRR is blue shifted by about 1nm primarily due to the resonator's effective index's change in the coupling region resulting from the change in its dimensions.

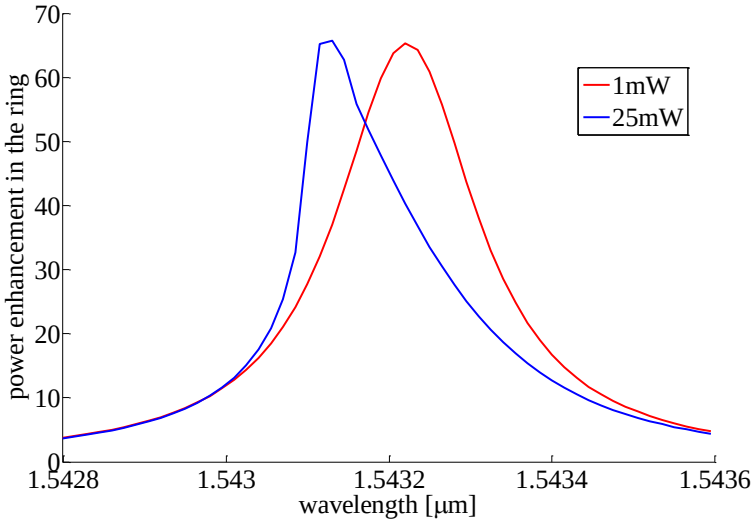

Figure 4.13: Tuning the MRR using the optomechanical effect. The power enhancement in the resonator near resonance is shown for the suggested device, at two power levels in the WG.

As was predicted already in sec. 4.4, the total force enhancement is quite moderate, and as a direct result the device's tunability is relatively low compared with novel structures that have been demonstrated theoretically and even experimentally [1]. Reasonable tunability can be achieved in our system only if we enlarge the GOF by feeding the WG with higher power. However, there is a limit to the optical power in the Si WG primarily because of the two-photon absorption process. The example of 50mW given here is not far from this limit. Alternatively, going to smaller separation gaps will lead to higher GOF values but on the other hand will broaden the transmission spectrum (lower Q value), and thus the overall tunability will not deviate significantly from the value reported here.

The Interim conclusion is that the standard MRR cannot be considered as an efficient optomechanical device. We thus seek for a better solution, as discussed in the next chapter.

5. The perturbed MRR

5.1. Introduction

In the previous sections we demonstrated the enhancement of the GOF by the use of an MRR, combined with optimal selection of the phase shift between the light propagating in the MRR and in the bus WG. However, the force enhancement is moderate, and consequently its effect on the optical signal is relatively small. This is because the enhancement is limited to the MRR, while the forces are obtained by the combined effect of the fields in both the MRR and the bus WG.

In order to further enhance the GOF and increase its effect on the optical signal propagating in the structure, we next consider taking advantage of the slow light effect by adding a periodic perturbation to the bus WG. Specifically, we aim to operate in the vicinity of the band edge of the periodic structure, where the light experiences high group index. Simultaneously the parameters are chosen such that we operate at one of the resonances of the MRR.

The idea of utilizing the effect of slow light at the band edge to enhance optical forces has been recently utilized for enhancing the force between a free standing 1-D PhC bar and its underlying substrate [20]. In our work we apply this concept for the first time in combination with the MRR structure for enhancing the GOF.

We choose our periodic perturbation to be consisted of air holes that are fully etched into the Si WG. For hole diameter of 300 nm and periodicity of 415 nm we found the first band edge to be around the telecom wavelength of $\lambda = 1.55\ \mu m$. The group index at each optical frequency is calculated from the dispersion diagram using

(5.1) $$n_g = c \cdot \left(\frac{\partial \omega}{\partial k}\right)^{-1}.$$

The force is expected to increase with the group index enhancement, which in turn corresponds to the obtained group index normalized by the group index of an unperturbed WG (~4 for the Si WG).

5.2. The relation between the force and the group index

We now validate the relation between the force enhancement and the slow light by calculating the GOF in a structure consisting of 2 perturbed WGs with respect to a structure of 2 unperturbed WGs. The double PhC WG structure exhibits a splitting in its dispersion diagram, corresponding to the symmetric and the anti-symmetric modes. Figure 5.1(a) shows the group index as a function of wavelength for the single PhC WG and the double PhC WG, together with the corresponding mode profiles. Figure 5.1(b) shows the force enhancement in the PhC structure. This is done by calculating the GOF using the MST and then normalizing it by the GOF in the unperturbed case of 2 slabs, as was calculated previously, for example in sec. 4.2.

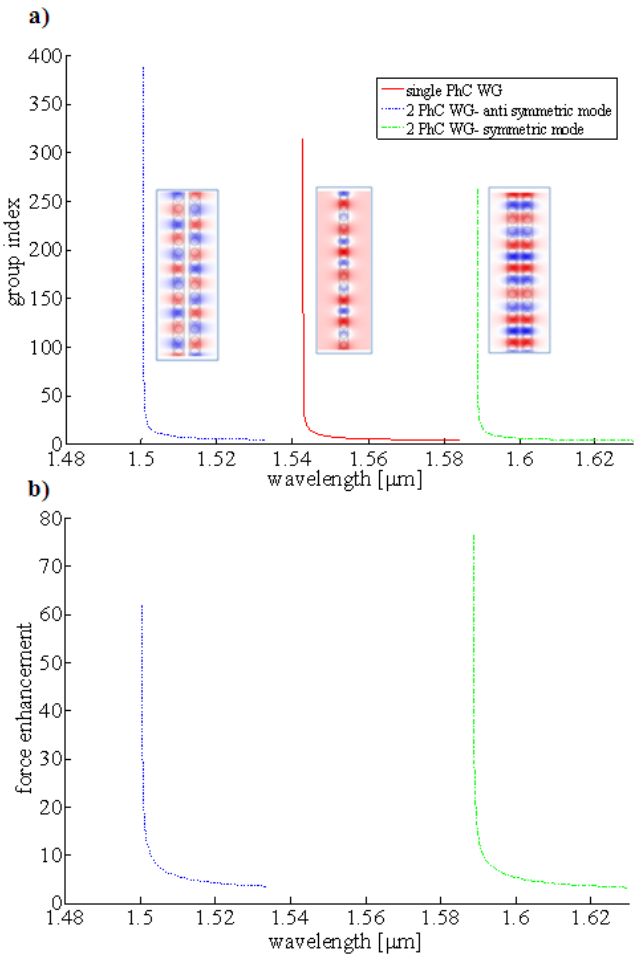

Figure 5.1: The Photonic-Crystal WG. (a) The group index in the vicinity of the first band edge is plotted as a function of the wavelength. Two structures are considered as shown in the insets with the electric field mode superimposed. 1-single silicon WG with periodic perturbation of air holes (data can be found in the sec. 5.1) and 2- two coupled silicon WGs with periodic perturbation of holes. (b) The force obtained in the periodically perturbed double WG system, normalized by the value obtained in the equivalent unperturbed structure.

As expected, the force is enhanced dramatically as the wavelength approaches the band edge, and the enhancement factor is close to the enhancement of the group index. The slight discrepancy between the group index enhancement and the force enhancement may be attributed to variation in mode profile as the wavelength approaches the band edge, as well as to numerical inaccuracies in the proximity of the band edge, in particular in estimating the group index near the band edge.

5.3. The combined structure of the MRR and the PhC

After validating that the periodic perturbation enhances the GOF, we simulate the desired structure, consisting of a bus WG with 30 holes (with similar parameters as in the previous example) drilled into it. This bus WG is coupled to an MRR, as shown in Figure 5.2(a). The separation gap is 250 nm. This structure gives rise to the coupling between two resonators. The first resonator is the 1-D PhC WG, with the interfaces between its Bloch mode and the mode of the ridge WG serving as mirrors. Such structures were previously shown to be useful in enhancing the quality factor as a result of the high group index towards the band edge [43]. The other resonator is the MRR. Clearly, the goal is to match the resonance frequencies of these two resonators. To do so, we tune the effective refractive index of the MRR. As mentioned previously, this can be achieved e.g. by modifying the height or the width of the MRR WG. The transmission spectrum near the band edge is shown in Figure 5.2(b) as a function of the wavelength and the MRR refractive index.

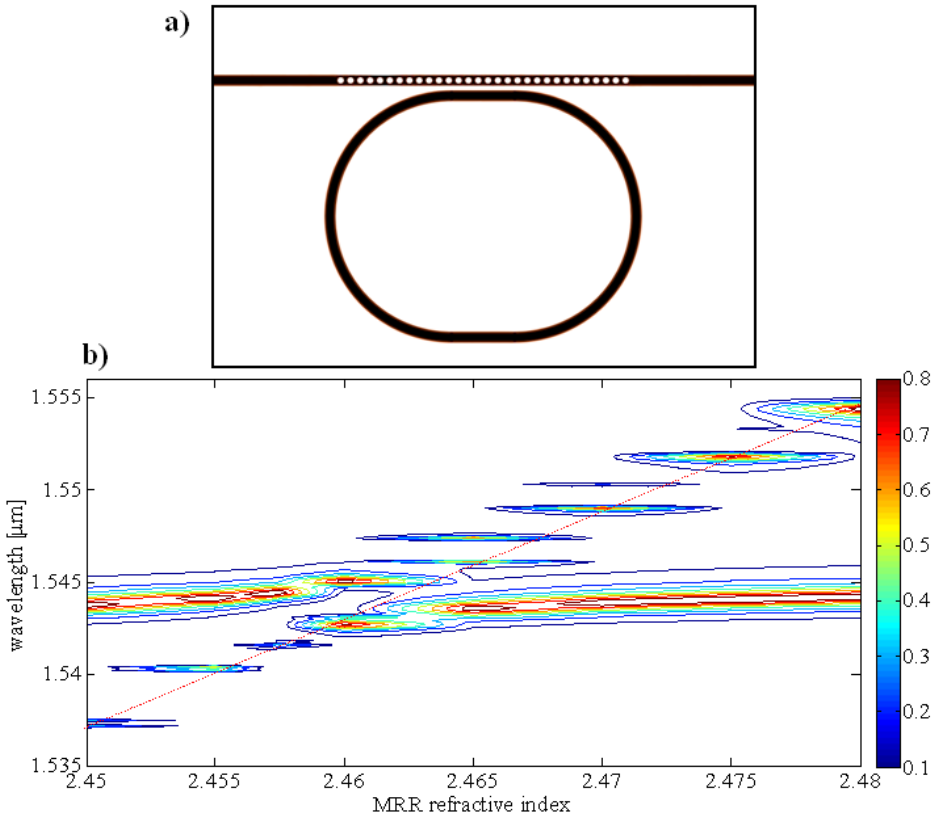

Fig. 5.2: The perturbed MRR system. (a) Drawing of the simulated structure, consisting of an MRR separated from a bus WG. Periodic perturbation of 30 air holes is embedded into the WG. The specific parameters are given in the text. (b) Transmission of light emerging from the structure of the MRR and a periodically perturbed bus WG as a function of the incident wavelength and the MRR refractive index. Red dotted line represents the shift in resonance wavelength as a function of variations in the MRR refractive index.

By observing Figure 5.2(b) we can identify the two resonances. First, we notice a resonance close to $\lambda = 1.545\ \mu m$ which is almost not affected by the change in the MRR refractive index. Therefore, this resonance is attributed to the 1-D PhC resonator. Additionally, we identify another transmission peak, with its resonance wavelength depends linearly on the MRR refractive index. This transmission peak is due to the MRR resonance. At the intersection point (around $n_{MRR} = 2.46$) between the two resonances, a resonances splitting is obtained.

Naively, one would expect a maximal GOF value to be obtained where the PhC and the MRR experience resonance simultaneously. However, our simulations show that the maximal GOF value is obtained slightly below the intersection point, at $n_{MRR} = 2.4572$. This fact may be understood as a trade-off between the resonances

intersection on one hand and group index enhancement on the other hand.

The force and the transmission as a function of the wavelength for this optimal value are shown in Figure 5.3. As shown we obtain a maximal force of ~ $25[nN/(\mu m \cdot W)]$ implying an enhancement of ~ 35 compared with the 2 unperturbed WGs system with the equivalent parameters. Clearly, this is a significant enhancement factor which may provide decent tunability of the proposed device.

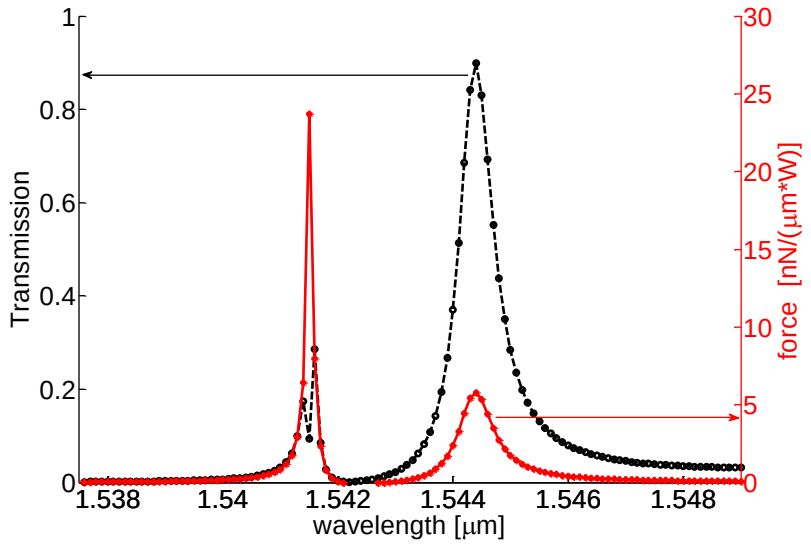

Figure 5.3: The transmission and the force acting on the WG are plotted against the wavelength, in the region next to the band edge. The refractive index of the MRR WG is assumed to be $n_{MRR} = 2.4572$.

We should mention that a standing wave pattern is observed in the calculated EM field, probably due to the reflections from the interface between the perturbed and the non perturbed sections. Moreover, the GOF itself is alternating between positive and negative values. Yet, as was discussed in sec. 4.3, the mechanical behavior is barely affected by these changes and the reported force values that correspond to the average can be considered as a reliable value.

The prediction is that the tuning properties of this hybrid device should be improved compared to the results obtained in sec. 4.5. This is due to two main reasons: 1 - The actual force is larger, and 2 - the Q factor is higher, meaning that the linewidth is smaller and the effect of tuning on the transmission is enhanced.

6. Conclusions

We analyzed the GOF acting on a bus WG coupled to an MRR, using the CMT and a numerical FEM. Our analytical model shows that the resonance enhancement of the force as a result of the MRR's power enhancement is diminished by the opposing contributions of the attractive and the repulsive forces related to the symmetric and the anti-symmetric modes in the coupling region. We suggested that adding asymmetry to the system by changing one of the WGs removes this restriction. By this procedure, we are able to demonstrate GOF of $F_{\max} \cong 7[nN/(\mu m \cdot W)]$ in an MRR with a reasonable Q factor of 10,000. This value corresponds to force enhancement of about an order of magnitude. Yet, the obtained GOF and the resultant optomechanical tunabilty are not utilizing the full power enhancement of the MRR since the field in the bus WG is not enhanced at all. As an improvement, we proposed adding a periodic perturbation to the bus WG in order to create a one dimensional PhC WG, and operating at the slow light regime. By this procedure and by careful matching between the MRR and the PhC resonances, this modified geometry allows further enhancement of the GOF (of about 35) via the combination of optical resonances and slow light effect.

Few future directions can be considered: firstly, the entire treatment is totally constant in time (up to the optical frequency). A more complete theoretical research should examine the time evolution of such a system, especially regarding the mutual relation of the mechanical and the EM effects. Secondly, we did not consider the thermal aspects of high optical powers (which are required in this kind of a device). These can add effects such as the thermo-elastic or thermo-optic. Finally, the novel structure of the MRR coupled to the 1-D PhC should be investigated more intensively and rigorously to understand the physical behavior of such a device.

List of abbreviations

EM	Electromagnetic
FEM	Finite-Element Method
GOF	Gradient Optical Force
INP	In-Plane (polarization)
MRR	Micro Ring Resonator
MST	Maxwell Stress Tensor
OOP	Out-Of-Plane (polarization)
PhC	Photonic Crystal
TE	Transverse Electric
TM	Transverse Magnetic
WG	Waveguide

Bibliography

1. D. Van Thourhout and J. Roels, "Optomechanical device actuation through the optical gradient force", Nature Photon. 4, 211-217 (2010).
2. J. Ng, C.T. Chan and P. Sheng, "Strong optical force induced by morphology-dependent resonances", Opt. Lett. 30, 1956-1958 (2005).
3. M. L. Povinelli, S. G. Johnson, M. Lončar, M. Ibanescu, E. J. Smythe, F. Capasso, and J. D. Joannopoulos, "High-Q enhancement of attractive and repulsive optical forces between coupled whispering-gallery-mode resonators", Opt. Express, 13, 8286-8295 (2005).
4. M. L. Povinelli, M. Lončar, M. Ibanescu, E. J. Smythe, S. G. Johnson, F. Capasso, and J. D. Joannopoulos, "Evanescent-wave bonding between optical waveguides", Opt. Lett. 30, 3042-3044 (2005).
5. A. Mizrahi and L. Sch¨achter, "Mirror manipulation by attractive and repulsive forces of guided waves", Opt. Express 13, 9804-9811 (2005).
6. A. Mizrahi and L. Sch¨achter, "Two-slab all-optical spring", Opt. Lett. 32, 692-694 (2007).
7. P. T. Rakich, M. A. Popovic, M. Soljacic, and E. P. Ippen, "Trapping, corralling and spectral bonding of optical resonances through optically induced potentials", Nature Photon. 1, 658-665 (2007).
8. F. Riboli, A. Recati, M. Antezza, and I. Carusotto, "Radiation induced force between two planar waveguides", The Eur. Phys. J.D 46, 157-164 (2008).
9. W.H.P. Pernice, M. Li and H.X. Tang, "Theoretical investigation of the transverse optical force between a silicon nanowire and a substrate", Opt. Express 17, 1806-1816 (2009).
10. W. H. P. Pernice, M. Li, K. Y. Fong, and H. X. Tang, "Modeling of the optical force between propagating lightwaves in parallel 3D waveguides", Opt. Express 17, 16032-16037 (2009).
11. L. Zhu, "Frequency dependence of the optical force between two coupled waveguides", Opt. Lett. 34, 2870-2872 (2009).

12. W.H.P. Pernice, M. Li and H.X. Tang , "A mechanical kerr effect in deformable photonic media", Appl. Phys. Lett. 95, 123507 (2009).
13. J. Ma and M.L. Povinelli, "Large tuning of birefringence in two strip silicon waveguides via optomechanical motion", Opt. Express 17, 17818-17828 (2009).
14. P. T. Rakich, M. A. Popovic and Z. Wang, "General Treatment of Optical Forces and Potentials in Mechanically Variable Photonic Systems", Opt. Express 17, 18116-18135 (2009).
15. A. Mizrahi, K. Ikeda, F. Bonomelli, V. Lomakin, and Y. Fainman, "Self-alignment and instability of waveguides induced by optical forces", Phys. Rev. A 80, 041804(R) (2009).
16. V. Liu, M. Povinelli, and S. Fan, "Resonance-enhanced optical forces between coupled photonic crystal slabs", Opt. Express 17, 21897-21909 (2009).
17. S. Huang and G.S. Agrawal, "reactive Coupling Induced Normal Mode Splittings in Microdisk Resonators Coupled to Waveguides", Phys. Rev. A 81, 053810 (2010).
18. C. Huang and L. Zhu, "Enhanced optical forces in 2D hybrid and plasmonic waveguides", Opt. Lett. 35, 1563-1565 (2010).
19. W.H.P. Pernice, M. Li, D. Garcia-Sanchez and H. X. Tang, "Analysis of short range forces in optomechanical devices with a nanogap", Opt. Express 18, 12615-12621 (2010).
20. J. Ma and M. L. Povinelli, "Effect of periodicity on optical forces between a one-dimensional periodic photonic crystal waveguide and an underlying substrate", Appl. Phys. Lett. 97, 151102 (2010).
21. R. Zhao, P. Tassin, T. Koschny and C. M. Soukoulis, "Optical forces in nanowire pairs and metamaterials", Opt. Express 18, 25665-25676 (2010).
22. M. Li, W. H. P. Pernice, C. Xiong, T. Baehrs-Jones, M. Hochberg, and H. X. Tang, "Harnessing optical forces in integrated photonic circuits", Nature 456, 480-484 (2008).
23. M. Li, W. H. P. Pernice and H.X. Tang, "Tunable bipolar optical interactions between guided lightwaves", Nature Phot. 3, 464-468 (2009).
24. J. Roels, I. De Vlaminck, L. Lagae, B. Maes, D. Van Thourhout and R. Baets, "Tunable optical forces between nanophotonic waveguides", Nature Nanotech. 4, 510-513 (2009).

25. W. H. P. Pernice, M. Li and H.X. Tang, "Optomechanical coupling in photonic crystal supported nanomechanical waveguides", Opt. Express 17, 12424-12432 (2009).
26. J. Rosenberg, Q. Lin and O. Painter, "Static and dynamic wavelength routing via the gradient optical force", Nature Phot. 3, 478-483 (2009).
27. G. S. Wiederhecker, L. Chen, A. Gondarenko and M. Lipson, "Controlling photonic structures using optical forces", Nature 462, 633 (2009).
28. G. S. Wiederhecker, S. Manipatruni, S. Lee and M. Lipson, "broadband tuning of optomechanical cavities", Opt. Express 19, 2782-2790 (2011).
29. M. Eichenfeld, C. P. Michael, R. Perahia and O. Painter, "Actuation of micro-optomechanical systems via cavity-enhanced optical dipole forces", Nature Photon. 1, 416-422 (2007).
30. M. Li, W. H. P. Pernice and H.X. Tang, "Reactive Cavity Optical Force on Microdisk-Coupled Nanomechanical Beam Waveguides", Phys. Rev. Lett. 103, 223901 (2009).
31. J. Chan, M. Eichenfield, R. Camacho and O. Painter, "Optical and mechanical design of a "zipper" photonic crystal optomechanical cavity", Opt. Express 17, 3802-3817 (2009).
32. M. Eichenfield, R. Camacho, J. Chan, K. J. Vahala and O. Painter, "A picogram- and nanometer-scale photonic-crystal optomechanical cavity", Nature 459, 550-555 (2009).
33. M. Eichenfield, J. Chan, R. Camacho, K. J. Vahala and O. Painter, "Optomechanical crystals", Nature 462, 78-82 (2009).
34. Q. Lin, J. Rosenberg, D. Chang, R. Camacho, M. Eichenfield, K. J. Vahala and O. Painter, "Coherent mixing of mechanical excitations in nano-optomechanical structures", Nature Phot. 4, 236-242 (2010).
35. Y.G. Roh, T. Tanabe, A. Shinya, H. Taniyama, E. Kuramochi, S. Matsuo, T. Sato, and M. Notomi, "Strong optomechanical interaction in a bilayer photonic crystal", Phys. Rev. B. 8, 121101(R) (2010).
36. T. P. M. Alegre, R. Perahia, and O. Painter, "Optomechanical zipper cavity lasers: theoretical analysis of tuning range and stability", Opt. Express 18, 7872-7885 (2010).

37. A. H. Safavi-Naeini, T. P. M. Alegre, M. Winger and O. Painter, "Optomechanics in an ultrahigh-Q two-dimensional photonic crystal cavity", App. Phys. Lett. 97, 181106 (2010).
38. J. D. Jackson, "Classical Electrodynamics", 3rd ed. (Wiley, 1998), Chap. 6.7.
39. A. Yariv, "Universal relations for coupling of optical power between microresonators and dielectric waveguides", Electronics Letters 36, 321-322 (2000).
40. K. Okamoto, "fundamentals of optical waveguides", 2nd ed. (Elsevier, 2006), Chap. 2.2.
41. H. Kogelnik, "Topics in Applied Physics" (Springer-Verlag, 1975), Vol. 7, Chap. 2.
42. I. Kiyat, A. Aydinli, and N. Dagli, "High-Q silicon-on-insulator optical rib waveguide racetrack resonators," Opt. Express 13, 1900-1905 (2005).
43. D. Goldring, U. Levy, I. Dotan, A. Tsukernik, M. Oksman, I. Rubin, Y. David, and D. Mendlovic, “Experimental measurement of quality factor enhancement using slow light modes in one dimensional photonic crystal,” Opt. Express 16, 5585-5595 (2008).

תקציר:

תחום הננו-פוטוניקה הינו תחום מדעי חדש יחסית המשלב את יכולות הייצור שנרכשות במדעי המיקרו-אלקטרוניקה אל תוך המערכות הפיסיקליות של האופטיקה והפוטוניקה. בשנים האחרונות מתעורר תת-תחום הבוחן את השפעתם של כוחות אופטיים על המבנים בהם זורם האור. כוח אופטי הינו למעשה כוח שמפעיל השדה האלקטרומגנטי על הסביבה. תת תחום זה מקבל משמעויות מעשיות שכן יכולות הייצור כיום מאפשרות בניית מבנים מורכבים בגדלים של מיקרומטר ואף פחות מכך כאשר חלק מהמבנה חופשי לנוע. יותר מכך, בגדלים כה קטנים, הכוחות האופטיים שבדרך כלל אין באפשרותנו לחוש אותם או להבחין בהשפעתם, יוצרים שינוי גיאומטרי של ממש.

בעבודה זו ביקשנו לחקור באופן תיאורטי את הכוח האופטי הנוצר במערכת ספציפית אשר מהווה אבן בניין בכל תחומי הפוטוניקה (חישה אופטית, תקשורת אופטית, אפנון ועוד)- המהוד הטבעתי. למהוד זה התנהגות אופיינית של העברת האות או הגברתו באופן צר סרט בתחום התדר. הציפייה, אם כן, היא כי בתנאי תהודה הגבר השדה החזק הנוצר בתוך הטכעת יוביל להגבר הכוח האופטי המופעל על מנחה הגל הצמוד למהוד (ומשמש לו כמזין). כוח זה יעוות במקצת את צורת מנחה הגל המזין ובכך תשתנה ההתנהגות האופטית של המערכת התלויה באופן משמעותי בגיאומטרייה של המבנה.

פיתחנו מודל תיאורטי המשתמש בתורת האופנים המצומדים על מנת להעריך את הכוח. מודל זה חזה כי תחת תנאים רגילים (בהם הטבעת עשויה מאותו מנחה גל של המנחה המזין)הכוח איננו מיטבי, וזאת לאור העובדה שהכוח איננו תלוי רק במשרעת השדות הנוצרת אלא גם בזווית המופע שבין השדות שבשני מנחי הגל. ביצענו הדמיות אלקטרומגנטיות מלאות של המערכת שאישרו את הממצאים. ביצענו הדמיות נוספות על מנת להעריך את המצב המיטבי אליו יש להביא את המערכת מבחינת ערכי הכוח המצופים. הראנו כי ערכי הכוח הגבוהים ביותר שניתן להגיע אליהם אינם גבוהים בהשוואה לעבודות אחרות בתחום, לאור העובדה שרק במהוד ישנו הגבר שדה משמעותי ולא במנחה הגל המזין. דבר זה מתבטא גם בעיוות הגיאומטרי הנוצר במערכת כתוצאה מהכוח- הדמיות המשלבות את ההתנהגויות הפוטונית והאלסטית על מנת לקבל את התנהגות המערכת הכוללת חוזות כי דרוש הספק גבוה למדי על מנת לקבל יכולת שליטה בתכונות המערכת. ניתן היה לסכם בכך את המחקר ולקבוע כי אכן התקן אופטו-מכני זה איננו יעיל.

עם זאת, הצענו גם דרך נוספת לשיפור וזאת על ידי הכנסת הפרעה מחזורית אל מנחה הגל המזין באיזור הצימוד לטבעת. הפרעה זו יוצרת תופעה של גביש פוטוני, כאשר בעבודתנו חיפשנו להתמקד בתנאים אשר יביאו לכך שהאור העובר במנחה הגל יחווה, בתדר מסויים, תופעה של "אור איטי"- מהירות החבורה של האור מונמכת באופן משמעותי עקב ההחזרות הנוצרות במבנה. תופעה זו גוררת עמה הגבר של השדה האלקטרומגנטי. בעבודתנו הראינו כי ניתן עקרונית לשלב הגבר זה יחד עם ההגבר הקיים בטבעת בכדי להגביר סימולטנית את כל האור הזורם ובכך לקבל ערכי כוח גבוהים יותר.